JCI The Journal of Clinical Investigation

Isocitrate-to-SENP1 signaling amplifies insulin secretion and rescues dysfunctional β cells

Mourad Ferdaoussi, Xiaoqing Dai, Mette V. Jensen, Runsheng Wang, Brett S. Peterson, Chao Huang, Olga Ilkayeva, Nancy Smith, Nathanael Miller, Catherine Hajmrle, Aliya F. Spigelman, Robert C. Wright, Gregory Plummer, Kunimasa Suzuki, James P. Mackay, Martijn van de Bunt, Anna L. Gloyn, Terence E. Ryan, Lisa D. Norquay, M. Julia Brosnan, Jeff K. Trimmer, Timothy P. Rolph, Richard G. Kibbey, Jocelyn E. Manning Fox, William F. Colmers, Orian S. Shirihai, P. Darrell Neufer, Edward T.H. Yeh, Christopher B. Newgard, Patrick E. MacDonald

J Clin Invest. 2015;125(10):3847-3860. https://doi.org/10.1172/JCI82498.

Research Article **Endocrinology**

Insulin secretion from β cells of the pancreatic islets of Langerhans controls metabolic homeostasis and is impaired in individuals with type 2 diabetes (T2D). Increases in blood glucose trigger insulin release by closing ATP-sensitive K^+ channels, depolarizing β cells, and opening voltage-dependent Ca^{2+} channels to elicit insulin exocytosis. However, one or more additional pathway(s) amplify the secretory response, likely at the distal exocytotic site. The mitochondrial export of isocitrate and engagement with cytosolic isocitrate dehydrogenase (ICDc) may be one key pathway, but the mechanism linking this to insulin secretion and its role in T2D have not been defined. Here, we show that the ICDc-dependent generation of NADPH and subsequent glutathione (GSH) reduction contribute to the amplification of insulin exocytosis via sentrin/SUMO-specific protease-1 (SENP1). In human T2D and an in vitro model of human islet dysfunction, the glucose-dependent amplification of exocytosis was impaired and could be rescued by introduction of signaling intermediates from this pathway. Moreover, islet-specific *Senp1* deletion in mice caused impaired glucose tolerance by reducing the amplification of insulin exocytosis. Together, our results identify a pathway that links glucose metabolism to the amplification of insulin secretion and demonstrate that restoration of this axis rescues β cell function in T2D.

Isocitrate-to-SENP1 signaling amplifies insulin secretion and rescues dysfunctional β cells

Mourad Ferdaoussi,[1,2] Xiaoqing Dai,[1,2] Mette V. Jensen,[3] Runsheng Wang,[4] Brett S. Peterson,[3] Chao Huang,[4] Olga Ilkayeva,[3] Nancy Smith,[1,2] Nathanael Miller,[5] Catherine Hajmrle,[1,2] Aliya F. Spigelman,[1,2] Robert C. Wright,[1,2] Gregory Plummer,[1,2] Kunimasa Suzuki,[1] James P. Mackay,[2] Martijn van de Bunt,[6] Anna L. Gloyn,[6,7] Terence E. Ryan,[8] Lisa D. Norquay,[9,10] M. Julia Brosnan,[10] Jeff K. Trimmer,[11] Timothy P. Rolph,[10] Richard G. Kibbey,[12] Jocelyn E. Manning Fox,[1,2] William F. Colmers,[2] Orian S. Shirihai,[5,13] P. Darrell Neufer,[8] Edward T.H. Yeh,[4] Christopher B. Newgard,[3] and Patrick E. MacDonald[1,2]

[1]Alberta Diabetes Institute and [2]Department of Pharmacology, University of Alberta, Edmonton, Alberta, Canada. [3]Sarah W. Stedman Nutrition and Metabolism Center and Duke Molecular Physiology Institute, Departments of Pharmacology and Cancer Biology and Medicine, Duke University, Durham, North Carolina, USA. [4]Department of Cardiology, The University of Texas MD Anderson Cancer Center, University of Texas, Houston, Texas, USA. [5]Department of Medicine, Boston University School of Medicine, Boston, Massachusetts, USA. [6]Oxford Centre for Diabetes, Endocrinology and Metabolism and [7]Oxford National Institute for Health Research Biomedical Research Centre, Churchill Hospital, Oxford University, Oxford, United Kingdom. [8]East Carolina Diabetes and Obesity Institute, Department of Physiology, East Carolina University, Greenville, North Carolina, USA. [9]Cardiovascular and Metabolic Research, Janssen Research and Development, Spring House, Pennsylvania, USA. [10]Cardiovascular and Metabolic Disease Department, Pfizer Research and Development, Cambridge, Massachusetts, USA. [11]Edison Pharmaceuticals Inc., Mountain View, California, USA. [12]Yale School of Medicine, Departments of Internal Medicine and Cellular and Molecular Physiology, New Haven, Connecticut, USA. [13]National Institute for Biotechnology in the Negev, Ben-Gurion University of the Negev, Be'er-Sheva, Israel.

Insulin secretion from β cells of the pancreatic islets of Langerhans controls metabolic homeostasis and is impaired in individuals with type 2 diabetes (T2D). Increases in blood glucose trigger insulin release by closing ATP-sensitive K^+ channels, depolarizing β cells, and opening voltage-dependent Ca^{2+} channels to elicit insulin exocytosis. However, one or more additional pathway(s) amplify the secretory response, likely at the distal exocytotic site. The mitochondrial export of isocitrate and engagement with cytosolic isocitrate dehydrogenase (ICDc) may be one key pathway, but the mechanism linking this to insulin secretion and its role in T2D have not been defined. Here, we show that the ICDc-dependent generation of NADPH and subsequent glutathione (GSH) reduction contribute to the amplification of insulin exocytosis via sentrin/SUMO-specific protease-1 (SENP1). In human T2D and an in vitro model of human islet dysfunction, the glucose-dependent amplification of exocytosis was impaired and could be rescued by introduction of signaling intermediates from this pathway. Moreover, islet-specific *Senp1* deletion in mice caused impaired glucose tolerance by reducing the amplification of insulin exocytosis. Together, our results identify a pathway that links glucose metabolism to the amplification of insulin secretion and demonstrate that restoration of this axis rescues β cell function in T2D.

Introduction

Insulin secretion from β cells of the pancreatic islets of Langerhans is impaired in type 2 diabetes (T2D) (1). The mechanism by which glucose elicits insulin secretion from β cells involves at least two key pathways (2). A metabolism-dependent closure of ATP-sensitive K^+ (K_{ATP}) channels (3, 4) elicits action potential firing (5) and activates voltage-dependent Ca^{2+} channels (VDCCs) (6) to trigger the Ca^{2+}-dependent exocytosis of insulin granules (7, 8). Seminal studies in the 1990s demonstrated an additional "K_{ATP}-independent" or "amplifying" action of glucose that is required for optimal secretion (9–11) and controls the amplitude of the secretory response (2). The prevailing evidence suggests that this metabolic amplification of insulin secretion occurs distally in the secretory pathway, possibly at the exocytotic site (12–14).

Multiple metabolic pathways have emerged as potential amplifiers of insulin secretion (13). These include a glycerolipid/free fatty acid cycle (15), which generates monoacylglycerol as a coupling factor (16); a phosphoenolpyruvate and mitochondrial GTP–dependent pathway (17, 18); and so-called "pyruvate cycles" (19–21), which export reducing equivalents from the mitochondria to the cytosol. The mitochondrial export of citrate and isocitrate and subsequent engagement of isocitrate with the cytosolic $NADP^+$-dependent isocitrate dehydrogenase (IDH1, hereafter referred to as ICDc) has been shown to regulate insulin secretion (22, 23), but the metabolites generated by this pathway that engage with the

▶ Related Commentary: p. 3754

Authorship note: Mourad Ferdaoussi and Xiaoqing Dai contributed equally to this work.
Note regarding evaluation of this manuscript: Manuscripts authored by scientists associated with Duke University, The University of North Carolina at Chapel Hill, Duke-NUS, and the Sanford-Burnham Medical Research Institute are handled not by members of the editorial board but rather by the science editors, who consult with selected external editors and reviewers.
Conflict of interest: Lisa D. Norquay is an employee of Janssen. Jeff K. Trimmer is an employee of Edison Pharmaceuticals Inc. and a shareholder of Pfizer. M. Julia Brosnan and Timothy P. Rolph are employees and shareholders of Pfizer. Christopher B. Newgard is a consultant for the Pfizer Cardiovascular and Metabolic Diseases Research Unit. This work was funded in part by a grant from Pfizer.
Submitted: April 23, 2015; **Accepted:** July 24, 2015.
Reference information: *J Clin Invest*. 2015;125(10):3847–3860. doi:10.1172/JCI82498.

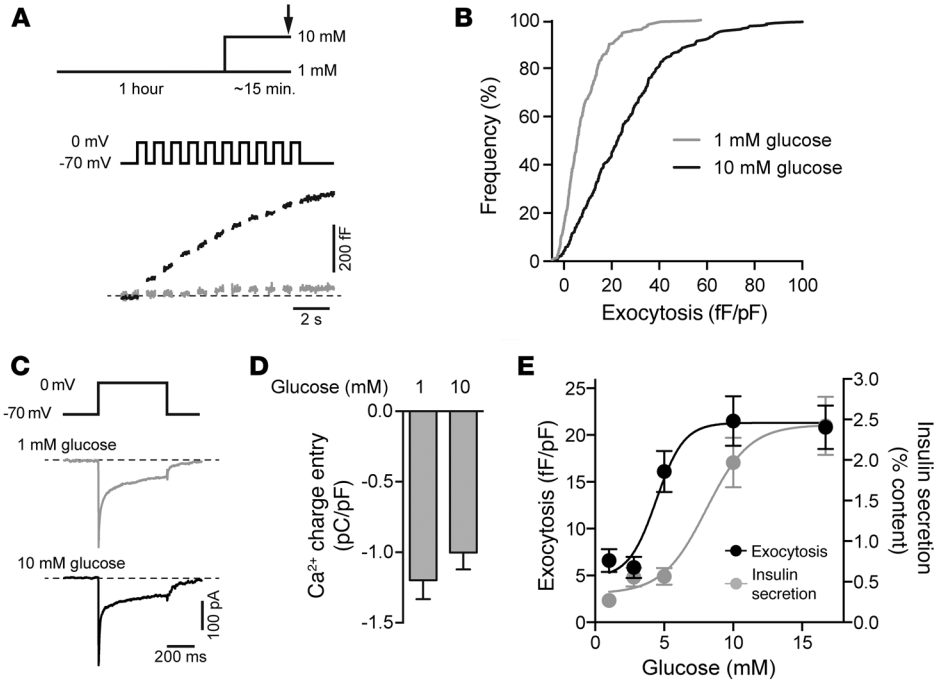

Figure 1. Glucose-dependent amplification of exocytosis in human β cells. (**A**) Exocytotic responses of single human β cells measured as increases in cell membrane capacitance by whole-cell patch clamp (at arrow) performed after acute pretreatment with 1 mM (gray trace) or 10 mM (black trace) glucose (representative of 280 and 311 cells from 50 donors). (**B**) Cumulative frequency distribution of the exocytotic response in β cells from 50 nondiabetic donors at 1 mM (*n* = 280 cells) and 10 mM glucose (*n* = 311 cells). (**C**) Representative voltage-activated Ca^{2+} currents from human β cells recorded at 1 mM and 10 mM glucose (representative of 72 and 79 cells from 14 donors). (**D**) The Ca^{2+} charge entry upon a single 500-ms depolarization to 0 mV at 1 mM (*n* = 72 cells; 14 donors) and 10 mM glucose (*n* = 79 cells; 14 donors). (**E**) The glucose concentration-response curve for amplification of the exocytotic response (black) of human β cells (*n* = 6 donors) is left-shifted compared with that for glucose-stimulated insulin secretion (gray) from intact human islets (*n* = 6 donors). Data are mean ± SEM and were compared by 2-tailed Student's *t* test.

insulin secretory machinery remain undefined. One possibility is that NADPH produced by ICDc may enhance insulin exocytosis via reduction of glutathione (GSH) and glutaredoxin-1 (GRX1) (24, 25). Additionally, whereas mitochondrial function is impaired in islets in T2D (26–28), the potential contribution of dysregulated pyruvate/isocitrate metabolism to impaired insulin exocytosis and insulin secretion has not been investigated in this setting.

SUMOylation refers to the covalent attachment of small ubiquitin-like modifier (SUMO) peptides to target proteins, which can modify protein subcellular localization and/or protein-protein interactions. SUMO peptides are removed by the sentrin/SUMO-specific proteases (SENPs) (29). The SUMO1 peptide can block insulin exocytosis at a distal step (30), and intriguingly, the activity of SENP1 may be redox sensitive (31), suggesting that it could transduce the GSH/GRX1 signal. Indeed, SENP1 alone can enhance insulin exocytosis, but this action is blocked under oxidizing conditions (32). SUMOylation may play diverse roles in pancreatic islet biology (33), having recently been implicated in metabolism (34), incretin receptor signaling (35), excitability (36), and survival (37). Importantly, the role for SENP1 in insulin secretion and in vivo glucose homeostasis remains to be resolved.

Here, we identified a mechanism responsible for amplification of the exocytotic response of human and rodent β cells. This pathway required isocitrate signaling through ICDc and the generation of NADPH and GSH as coupling factors that act through SENP1 to amplify insulin exocytosis. A role for islet SENP1 as a regulator of in vivo glucose homeostasis was demonstrated by the tissue-selective and inducible knockout of this enzyme. Finally, the glucose-dependent amplification of exocytosis was lost in human T2D β cells but could be rescued by several key intermediates from the proposed isocitrate-to-SENP1 pathway, thereby suggesting new targets for reversing islet dysfunction in T2D.

Results

The glucose-dependent amplification of exocytosis in human β cells is mimicked by metabolic signaling intermediates. Exocytosis in single human β cells, identified by insulin immunostaining, was amplified by glucose stimulation (Figure 1A). In this protocol, we preincubated β cells for 1 hour at low (1 mM) glucose and then stimulated them with 10 mM glucose for approximately 15 minutes, before whole-cell patch clamping to measure the exocytotic response triggered by direct membrane depolarization. This allowed us to measure the ability of prior glucose stimulation to amplify the subsequent exocytotic response. Compared with cells kept at 1 mM glucose, 10 mM glucose amplified the exocytotic response of β cells to membrane depolarization (Figure 1B) from an average of 8.3 ± 0.6 fF/pF to 26.3 ± 1.3 fF/pF (*n* = 280 and 311 cells from 50 donors, $P < 0.001$). This occurred without increasing Ca^{2+} current (Figure 1, C and D, and ref. 38) and is consistent with the view that glucose amplifies insulin exocytosis independent of plasma membrane potential (which was clamped) and Ca^{2+} influx (which was unchanged). The concentration dependence of this amplifying action of glucose was significantly ($P < 0.05$) left shifted (EC_{50} = 4.9 ± 0.4 mM, *n* = 6 donors) compared with its action on insulin secretion (EC_{50} = 7.2 ± 0.8 mM, *n* = 6 donors) of isolated human islets (Figure 1E), consistent with an amplifying pathway that operates at glucose levels below the 5 to 7 mM threshold for triggering insulin secretion (11).

We examined whether a pathway downstream of mitochondrial isocitrate export could replicate the amplifying action of glucose. The intracellular dialysis (Figure 2A) of 100 μM isocitrate (Figure 2B) amplified the exocytotic response of human β cells to the same extent as 10 mM glucose. The product of the ICDc reaction, α-ketoglutarate (α-KG; 100 μM), did not amplify exocytosis (Figure 2C), and a direct comparison in β cells from the same human donors showed clearly that isocitrate amplified the

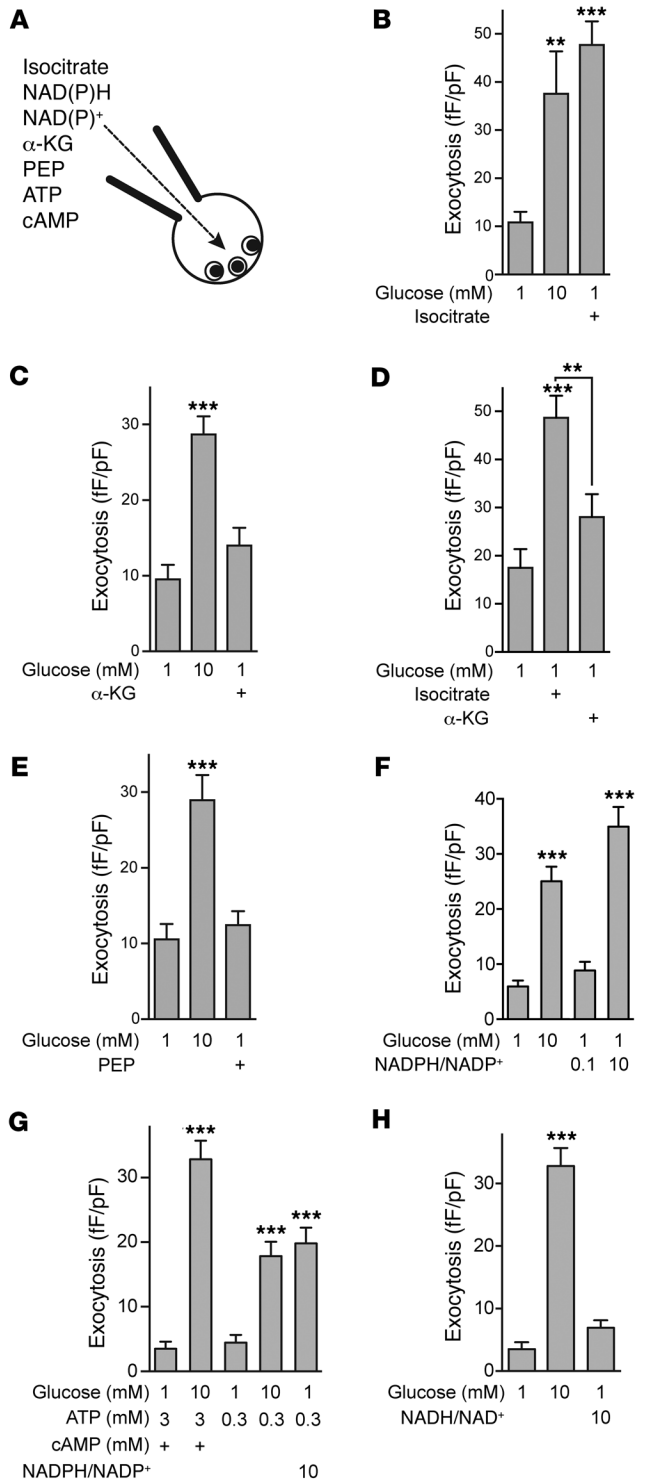

Figure 2. Intracellular delivery of metabolic coupling intermediates reveals a role for isocitrate-derived NADPH in the control of β cell exocytosis. (**A**) Illustration of the whole-cell patch-clamp for intracellular delivery of molecules prior to (~3 minutes) stimulation of exocytosis by membrane depolarization. (**B**–**E**) The total exocytotic response of human β cells following acute glucose (10 mM) pretreatment, as in Figure 1A, or upon infusion of (**B**) 100 μM isocitrate (*n* = 42, 15, 59 cells; 7 donors), (**C**) 100 μM α-KG (*n* = 20, 24, 26 cells; 3 donors), (**D**) comparing infusion of either 100 μM isocitrate or α-KG in the same donors (*n* = 28, 36, 35 cells; 4 donors), or (**E**) upon infusion of 100 μM phosphoenolpyruvate (PEP) (*n* = 28, 20, 35 cells; 4 donors). (**F**) The amplification of exocytosis from 1 mM (*n* = 33 cells; 4 donors) to 10 mM glucose (*n* = 15 cells; 3 donors) is replicated by direct intracellular dialysis of NADPH (in a 10:1 molar ratio with $NADP^+$, *n* = 34 cells, 4 donors compared with a ratio of 1:10, *n* = 31 cells, 4 donors). (**G**) As in **F**, without cAMP and with low (0.3 mM) ATP (*n* = 20, 24, 22, 23, 31 cells; 3 donors). (**H**) As in **F**, but with infusion of NADH (in a 10:1 molar ratio with NAD^+, *n* = 20, 24, 31 cells, 3 donors). *n* values correspond to graph bars from left to right, respectively. Data are mean ± SEM and were compared with ANOVA followed by Bonferroni post-test. $^{**}P < 0.01$, $^{***}P < 0.001$ compared with the 1 mM glucose condition, unless indicated otherwise.

exocytotic response, while α-KG did not (Figure 2D). The glycolytic intermediate phosphoenolpyruvate (100 μM) was also unable to amplify the exocytotic response of human β cells (Figure 2E). When isocitrate is converted to α-KG, NADPH is produced, and NADPH (10:1 with $NADP^+$, see Methods) amplified the exocytotic response and mimicked the effect of glucose (Figure 2F). Similar results were obtained using the rodent insulinoma cell line INS 832/13 (Supplemental Figure 1; supplemental material available online with this article; doi:10.1172/JCI82498DS1). Although the above experiments were all performed with 3 mM ATP and 0.1 mM cAMP in the patch pipette, NADPH remained able to amplify insulin exocytosis, even when cAMP was absent and ATP was low (0.3 mM) (Figure 2G). Finally, NADPH could not be replaced by NADH (at 10:1 ratio with NAD^+), which was unable to amplify the exocytotic response in human β cells (Figure 2H).

ICDc is required for the glucose- and isocitrate-dependent amplification of β cell exocytosis. Knockdown of ICDc in INS 832/13 cells completely blocked the amplification of exocytosis by 10 mM glucose, and this was rescued by intracellular application of NADPH (10:1 with $NADP^+$; Supplemental Figure 2, A and B). Similar experiments in human β cells showed that ICDc knockdown (Supplemental Figure 2C) impairs the amplification of exocytosis by 10 mM glucose (Figure 3A) or 100 μM isocitrate (Figure 3B) but not the response to NADPH (10:1 with $NADP^+$; Figure 3C). These findings are consistent with a requirement for ICDc to generate signals that amplify exocytosis and suggest that NADPH is the key coupling factor in this pathway.

The NADPH-dependent facilitation of insulin exocytosis may occur through its interaction with the glutathione/glutaredoxin system (25). In this model, cytosolic NADPH (but not NADH; refs. 39, 40) acts as a cofactor in the glutathione reductase reaction to maintain a pool of GSH, which, in turn, maintains GRX1 in a reduced state, allowing it to serve as a direct effector of granule exocytosis (24). Using a GSH biosensor (Grx1-roGFP) targeted to the cytosol, we found in human islets that glucose stimulation causes an increase in cytosolic GSH (i.e., a lowering of the oxidation state of this probe; Figure 3D). Since detection of glucose-dependent changes in cytosolic GSH within islets has been difficult using this method (41), we also used HPLC to resolve the reduced and oxidized forms of whole-cell glutathione (GSH and GSSG, respectively) in INS 832/13 cells (Figure 3, E–J). Glucose stimulation of INS 832/13 cells increased GSH (Figure 3, G–J), such that the ratio of GSH at stimulatory glucose to that of GSSG at basal glucose was clearly elevated (Figure 3, E–H), whereas GSSG levels were not changed at stimulatory compared to basal glucose (Figure 3, F–I). This increase in the GSH/GSSG ratio in response to stimulatory glucose was abrogated by ICDc

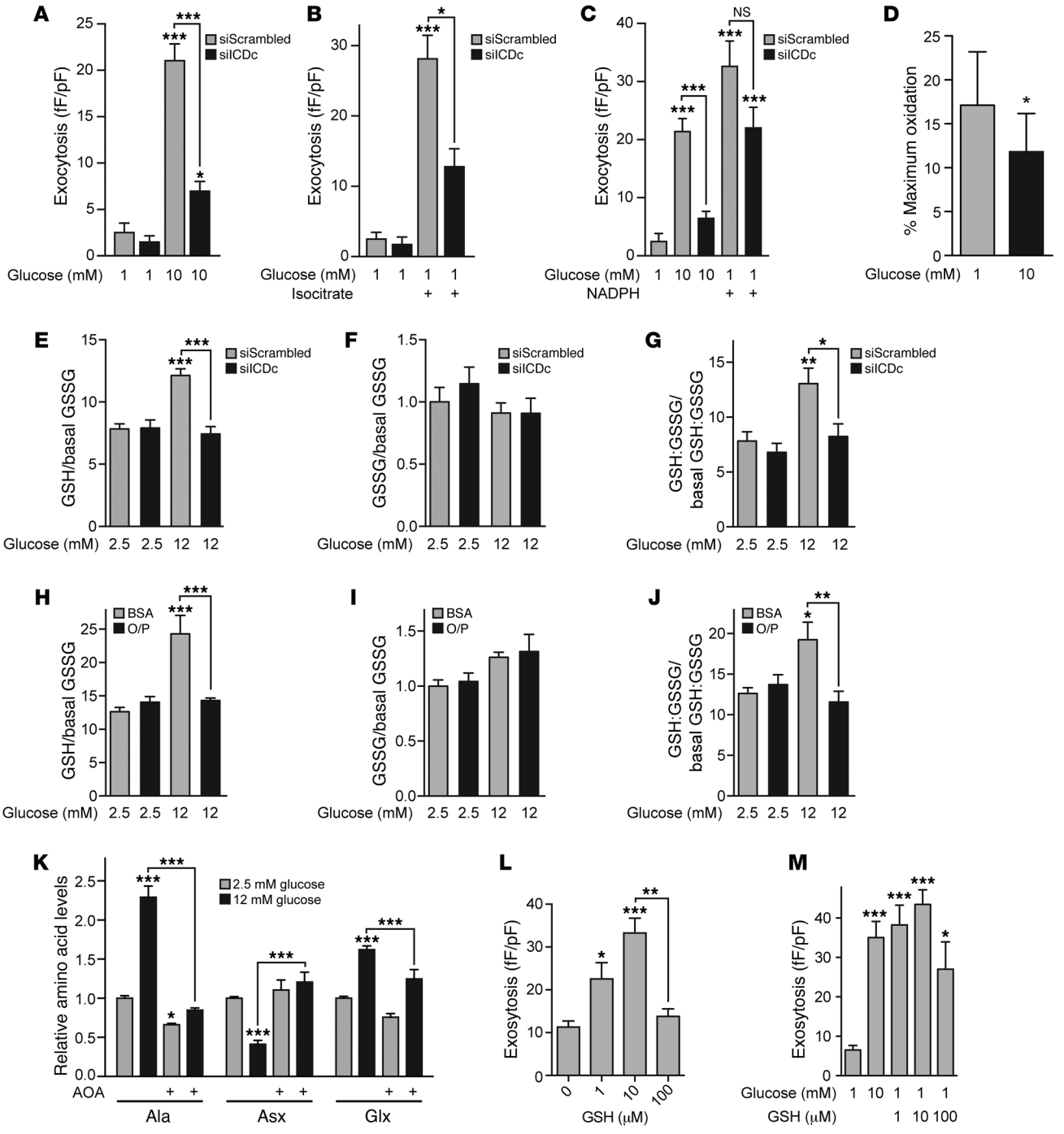

Figure 3. ICDc is required for glucose-dependent glutathione reduction and the amplification of β cell exocytosis. Knockdown of ICDc (siICDc) in human β cells blunts amplification of exocytosis by (**A**) glucose (10 mM; *n* = 24, 41, 18, 49 cells; 7 donors) or (**B**) isocitrate (100 μM; *n* = 16, 14, 10, 27 cells; 4 donors), (**C**) which was rescued by NADPH (10:1 with $NADP^+$; *n* = 16, 33, 29, 26, 31 cells; 5 donors). (**D**) Oxidation state of Grx1-roGFP expressed in reaggregated human islets (*n* = 7 donors). (**E** and **H**) Normalized to baseline GSSG, GSH is increased by glucose in INS 832/13 cells. (**F** and **I**) As GSSG is unchanged, (**G** and **J**) the ratio of reduced-to-oxidized glutathione (GSH:GSSG) is increased by glucose. Compared with siScrambled or BSA-treated controls, these responses are lost in INS 832/13 cells following (**E**–**G**) knockdown of ICDc (siICDc; *n* = 9 replicates in 3 experiments) or (**H**–**J**) 48-hour culture with 400 μM oleate/palmitate (O/P; *n* = 6 replicates in 2 experiments). (**K**) Measurement of amino acids in INS 832/13 cells reveals glucose-dependent increases in alanine (Ala) and glutamic acid/glutamine (Glx) and a drop in asparagine/aspartic acid (Asx), which are blocked by aminooxyacetic acid (AOA; *n* = 3 separate experiments). Intracellular dialysis of GSH amplified exocytosis in (**L**) INS 832/13 cells (*n* = 18, 12, 13, 12 cells) and (**M**) human β cells (*n* = 33, 24, 14, 49, 15 cells; 5 donors). Data are mean ± SEM and were compared with (**A**–**C**, **E**–**K**, and **M**) ANOVA followed by Bonferroni post-test, (**D**) Wilcoxon matched pairs test, or (**L**) with the nonparametric Kruskal-Wallis 1-way ANOVA followed by Dunn's post-test. *n* values correspond to graph bars from left to right, respectively. $^*P < 0.05$, $^{**}P < 0.01$, $^{***}P < 0.001$ compared with the control 1 mM glucose condition, unless indicated otherwise.

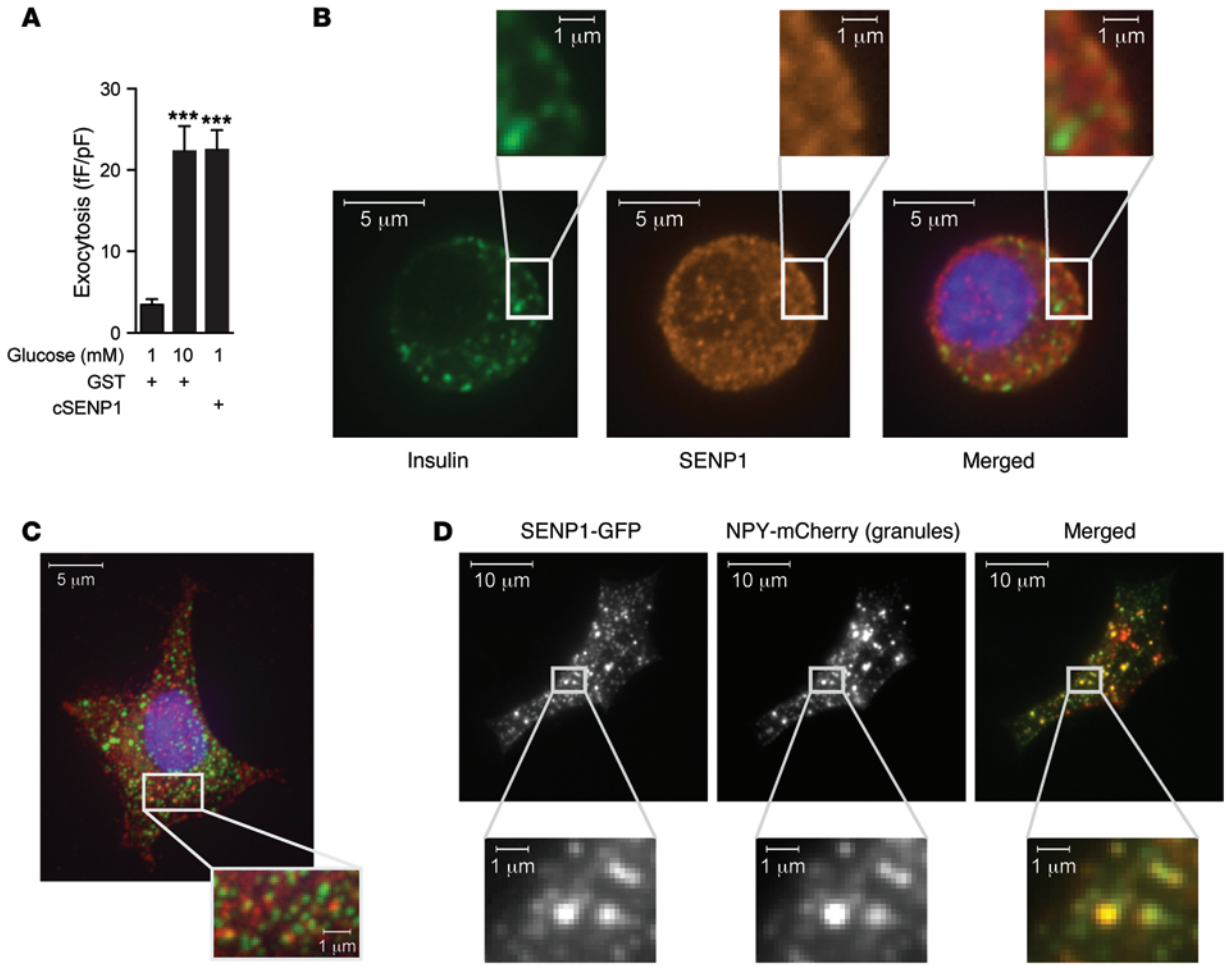

Figure 4. SENP1 expression in β cells. (**A**) The amplification of exocytosis from 1 to 10 mM glucose, with glutathione-*S*-transferase (GST) peptide infused as a control, was also mimicked by intracellular dialysis of cSENP1 (4 μg/ml; n = 33, 28, 45 cells, left to right, respectively; 4 donors). (**B** and **C**) Confocal imaging of (**B**) a human β cell (representative of 34 cells from 3 donors) and (**C**) a INS 832/13 cell (representative of 47 cells from 4 experiments) immunostained for insulin (green) and SENP1 (red). Nuclear staining is with DAPI (blue). (**D**) TIRF microscopy reveals that in INS 832/13 cells SENP1-EGFP and NPY-mCherry (granule marker) colocalize at the plasma membrane (representative of n = 35 cells; 5 experiments). Data are mean ± SEM and were compared with ANOVA followed by Bonferroni post-test. ***P < 0.001 compared with 1 mM glucose control. Scale bar: 1 μm (**B**–**D**, insets); 5 μm (**B** and **C**); 10 μm (**D**).

knockdown (Figure 3, E–G) or following culture of INS 832/13 cells under lipotoxic conditions (Figure 3, H–J).

In addition to serving as a source of NADPH, the pyruvate-isocitrate pathway may contribute to de novo glutathione biosynthesis. In INS 832/13 cells, measurement of amino acids by targeted tandem mass spectrometry revealed that levels of 13 of 16 amino acids were unchanged during glucose stimulation (data not shown). Of the remaining 3 amino acids, the glucose-dependent rise in alanine (Figure 3K) likely resulted from transamination of pyruvate by alanine transaminase. Interestingly, we also observed a glucose-dependent increase in glutamic acid and glutamine and a corresponding decrease in asparagine and aspartic acid (Figure 3K), consistent with a model whereby α-KG produced from the ICDc reaction engages with the cytosolic isoform of aspartate aminotransferase (GOT1) to transaminate α-KG to glutamate (Supplemental Figure 2D). This was blocked by the general transaminase inhibitor aminooxyacetic acid, which also impaired glucose-stimulated insulin secretion in both INS 832/13 cells and primary rat islets (data not shown). The glutamate produced by GOT1 was available for de novo synthesis of glutathione via condensation with cysteine (glutamate-cysteine ligase reaction) and then glycine (glutathione synthetase reaction; Supplemental Figure 2D) and may explain why glutamate also amplifies the β cell exocytotic response (42). Consistent with this, knockdown of ICDc decreased the total pool of glutathione (GSH plus GSSG) in INS 832/13 cells at stimulatory (12 mM) glucose concentrations, from 243.0 ± 22.7 to 165.7 ± 22.4 μmoles/mg protein (P < 0.05, n = 3 experiments).

Previous work demonstrated that GSH can produce a modest enhancement of exocytosis in rat β cells at 5 mM glucose, which is already near the threshold for insulin secretion (25). To test whether GSH is sufficient to amplify the exocytotic response, we examined whether intracellular application of GSH could amplify exocytosis under low glucose (1 mM). The exocytotic response was amplified by intracellular dialysis of GSH (1–100 μM) to the interior of INS 832/13 cells (Figure 3L) and human β cells (Figure 3M). Furthermore, intracellular infusion of 10 μM GSH remained able to amplify exocytosis following knockdown of ICDc (Supplemental Figure 2E).

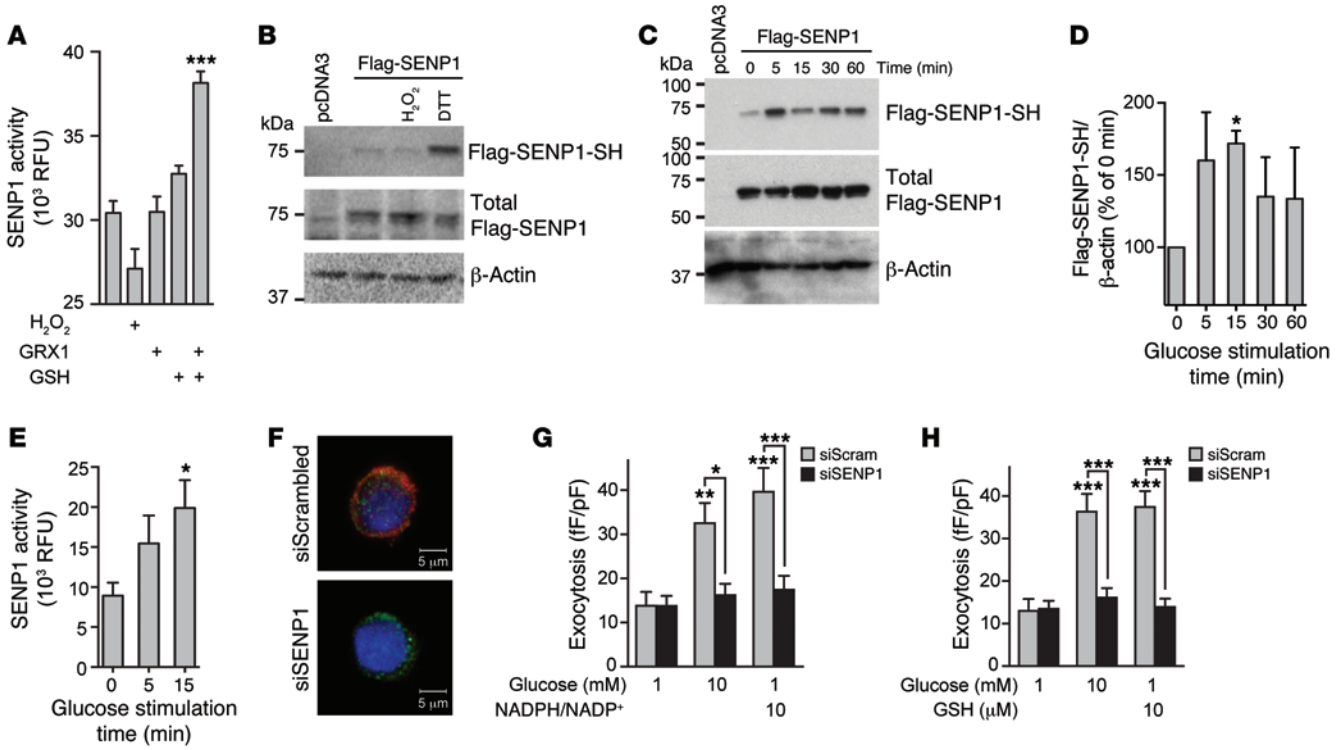

Figure 5. SENP1 couples redox state to insulin exocytosis. (**A**) The activity of cSENP1 is enhanced by GSH (10 μM), and this is facilitated by GRX1 (10 μg/ml; *n* = 3 experiments). (**B**) Reduction of thiol groups on recombinant Flag-SENP1 expressed in INS 832/13 cells (representative of 3 experiments). (**C** and **D**) Stimulation of INS 832/13 cells expressing Flag-SENP1 with 10 mM glucose demonstrates glucose-dependent reduction of SENP1 thiols. (**C**) A representative blot and (**D**) quantified data normalized to time = 0 (*n* = 5 experiments). (**E**) Native SUMO protease activity in INS 832/13 cells is increased following stimulation of cells with 10 mM glucose (*n* = 9 experiments). (**F**) Knockdown of SENP1 in human β cells (insulin, green; SENP1, red; DAPI, blue; representative of 19 and 14 cells) (**G**) prevents the amplification of exocytosis by NADPH (*n* = 22, 23, 22, 27, 25, 29 cells; 4 donors) and (**H**) GSH (*n* = 26, 28, 27, 36, 34, 44 cells; 5 donors). *n* values correspond to graph bars from left to right, respectively. Data are mean ± SEM and were compared with ANOVA followed by Bonferroni post-test. $^*P < 0.05$, $^{**}P < 0.01$, $^{***}P < 0.001$. Scale bar: 5 μm (**F**).

SENP1 amplifies exocytosis in β cells downstream of NADPH and GSH. SUMO1 acts as a brake on insulin exocytosis (30), and SENP1's catalytic activity is reportedly redox dependent (31). Intracellular application of the SENP1 catalytic domain (cSENP1; 4 μg/ml) mimicked the ability of glucose to amplify exocytosis in human β cells (Figure 4A) and rescued the exocytotic response of INS 832/13 cells following knockdown of ICDc (Supplemental Figure 2E). *SENP1* was expressed in human islets, and its mRNA level was unchanged in islets from donors with T2D (Supplemental Figure 3A). SENP1 protein colocalized with insulin granules in both human β cells (thresholded Pearson's coefficient of 0.61 ± 0.02; *n* = 34 β cells from 3 donors; Figure 4B) and INS 832/13 cells (thresholded Pearson's coefficient of 0.68 ± 0.01; *n* = 47 cells from 4 separate experiments; Figure 4C). Furthermore, when overexpressed in INS 832/13 cells, SENP1-GFP colocalized with secretory granules at the plasma membrane (thresholded Pearson's coefficient of 0.68 ± 0.04, *n* = 35 cells in 5 experiments; Figure 4D). No such membrane targeting of SENP1 was observed in HEK293 cells (data not shown).

The catalytic activity of cSENP1 was promoted by GSH and GRX1 (Figure 5A) and treatment of recombinant Flag-SENP1 with the reducing agent DTT exposed free thiols (Figure 5B), which are proposed to be required for SENP1 activity (31). Substitution of cysteines 603 and 613 (with serine) abolishes SENP1 enzymatic activity (43) and oxidation-induced disulfide-mediated dimerization (31) and prevented the SENP1-dependent amplification of exocytosis in INS 832/13 cells (Supplemental Figure 3, B and C). In addition, glucose stimulation (10 mM) exposed reduced thiols on Flag-SENP1 in INS 832/13 cells, with a maximum response at 15 minutes (Figure 5, C and D), and increased native SUMO protease activity (Figure 5E). Consistent with a key role for SENP1 in transducing the redox signal, knockdown of SENP1 in human β cells (Figure 5F and Supplemental Figure 3C) prevented the amplification of exocytosis by NADPH (10:1 with $NADP^+$; Figure 5G) or GSH (10 μM; Figure 5H). Thus, SENP1 can localize to secretory granules, including those at the plasma membrane. Its activity is enhanced by, and required for, redox signals downstream in the NADPH-dependent control of insulin exocytosis.

Glucose-dependent amplification of β cell exocytosis is impaired in T2D. Impaired insulin exocytosis is implicated in both in vitro (44) and in vivo (45) rodent models of diabetes, and reduced expression of the exocytotic SNARE proteins has been demonstrated in islets from a limited number of human donors with T2D (46). However, the mechanism underpinning reduced insulin secretion in T2D is unknown, and the connection between impaired mitochondrial function (27, 28, 47) and exocytotic efficiency is unclear. In an in vitro model of human islet dysfunction involving culture of islets with elevated free fatty acids (48), the glucose-dependent amplification of β cell exocytosis was blunted (Figure 6, A and B),

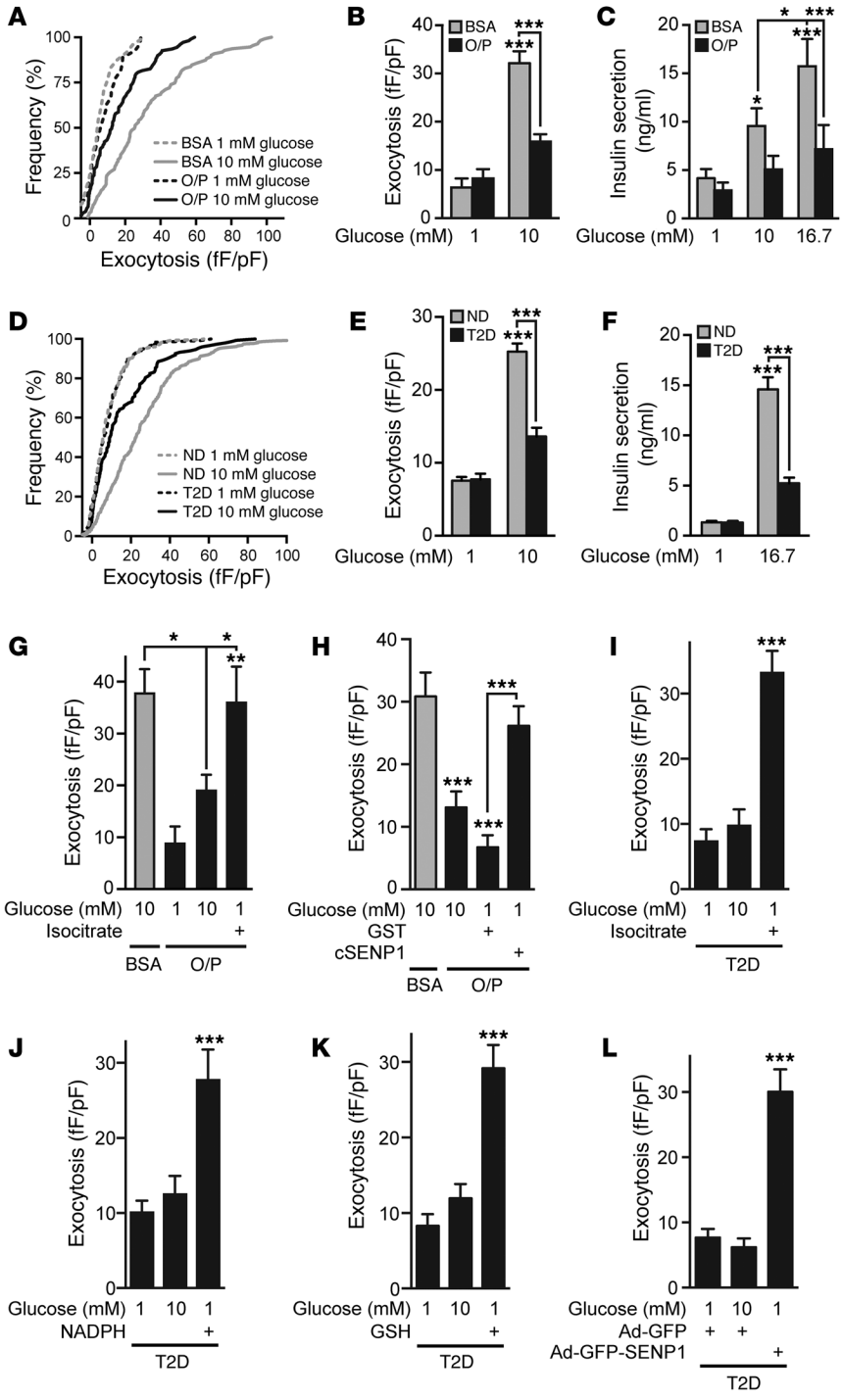

Figure 6. Glucose-dependent amplification of exocytosis in human β cells is impaired in T2D and rescued by activating the isocitrate-to-SENP1 pathway. (**A**) Cumulative frequency distribution of exocytotic responses from human β cells cultured under control conditions (BSA) or following 400 μM oleate/palmitate culture, after acute pretreatment with 1 or 10 mM glucose (n = 24, 56, 27, 65 cells; 6 donors). (**B**) Average exocytotic and (**C**) secretory responses of BSA-treated and oleate/palmitate-treated cells and islets (n = 5 donors), respectively. (**D**) Cumulative frequency distribution of exocytotic responses from human β cells from nondiabetic donors (ND, same as Figure 1B; n = 280, 311 cells; 50 donors) or donors with T2D (black lines; n = 116, 148 cells; 19 donors). (**E**) Average exocytotic and (**F**) secretory responses of nondiabetic and T2D cells and islets, respectively (for secretion, n = 28 nondiabetic and 12 donors with T2D). (**G** and **H**) Total exocytotic response of control treated (BSA) or oleate/palmitate-treated human β cells to glucose stimulation or infusion of (**G**) 100 μM isocitrate (n = 24, 12, 34, 26 cells; 3 donors) or (**H**) 4 μg/ml cSENP1 (n = 40, 37, 28, 41 cells; 5 donors). (**I**–**L**) Total exocytotic responses of β cells from donors with T2D following infusion of (**I**) 100 μM isocitrate (n = 25, 26, 47 cells; 4 donors), (**J**) NADPH (at 10:1 with $NADP^+$; n = 47, 41, 63 cells; 5 donors), or (**K**) 10 μM GSH (n = 29, 39, 50 cells; 4 donors), or (**L**) upon transduction with Ad-GFP or Ad-GFP-SENP1 (n = 31, 35, 51 cells; 4 donors). Data are mean ± SEM and were compared with ANOVA followed by Bonferroni post-test. $^*P < 0.05$, $^{**}P < 0.01$, $^{***}P < 0.001$. n values correspond to graph bars from left to right, respectively.

mirroring the impaired insulin secretory response (Figure 6C). In β cells from donors with T2D, glucose was likewise largely unable to amplify exocytosis (Figure 6, D and E). We also confirmed impaired insulin secretion in islets from several donors with T2D (Figure 6F). While glucose stimulation was ineffective, increasing either isocitrate or SENP1 rescued exocytosis in the in vitro model (Figure 6, G and H). Similarly, amplification of the exocytotic response in β cells from donors with T2D could be rescued by intracellular infusion of isocitrate (Figure 6I), NADPH (Figure 6J), or GSH (Figure 6K) or by upregulating SENP1 (Figure 6L). These data suggest that the glucose-dependent pathway for amplifying β cell exocytosis is impaired in T2D but can be rescued by several coupling factors generated along the isocitrate-to-SENP1 pathway.

Islet SENP1 regulates glucose homeostasis in vivo by controlling the glucose-dependent amplification of insulin secretion. Reduced expression of SENP1 in islet cells protects against apoptosis (37), while increasing SUMOylation may impair insulin secretion (30, 35). To determine the role of SENP1 in vivo, we generated *SENP1*$^{fl/fl}$ mice and crossed them with the *Pdx1-Cre* line (49) to generate a tissue-selective knockout (herein referred to as *p*SENP1-KO; Figure 7A) mice and with the *Pdx-CreER* line (50) to generate an inducible β cell–specific knockout (herein referred to as *i*βSENP1-KO)

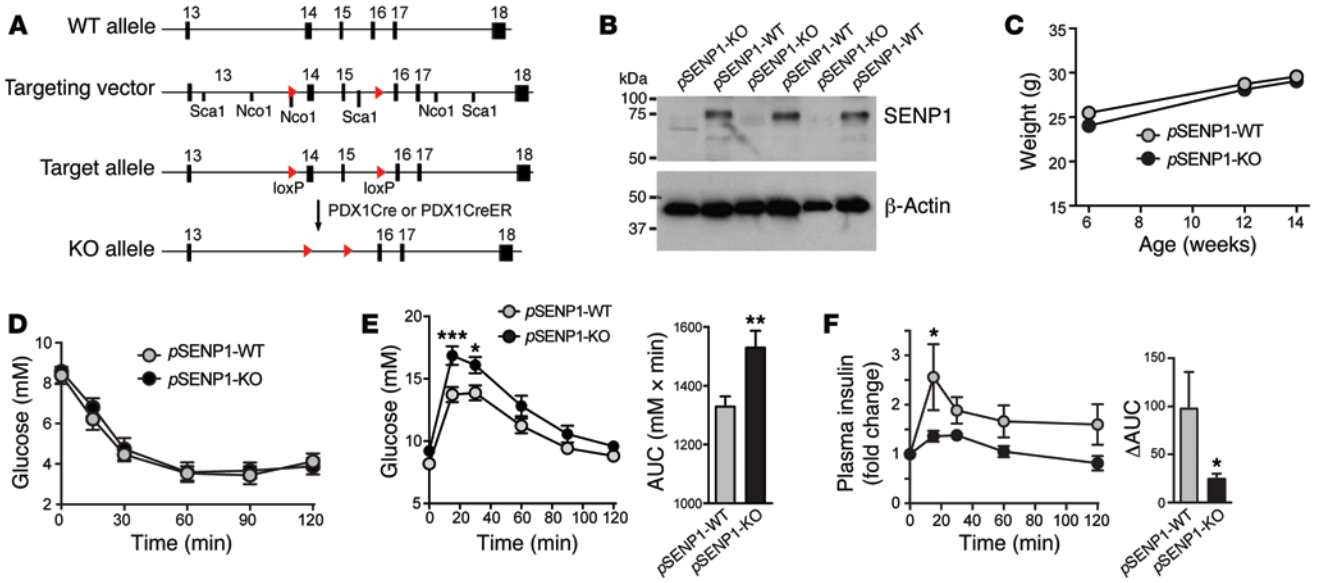

Figure 7. Pancreatic islet–selective knockout of *Senp1* in mice results in impaired glucose-tolerance and plasma insulin responses. (**A**) Illustration of the generation of tissue-selective knockout mice. To generate *SENP1*$^{fl/fl}$ mice, exons 14 and 15 of the *Senp1* gene were flanked by 2 loxP sequences. The *SENP1*$^{fl/fl}$ mice were then crossed with *Pdx1-Cre* or *Pdx1-CreER* lines to generate *p*SENP1-KO and *iβ*SENP1-KO mice, respectively. (**B**) SENP1 protein expression in islets from wild-type (*p*SENP1-WT) and *p*SENP1-KO mice (n = 3 mice of each genotype). (**C**) Body weight of *p*SENP1-WT (n = 18) and *p*SENP1-KO (n = 14) mice. (**D**) Insulin tolerance of the *p*SENP1-WT (n = 13) and *p*SENP1-KO (n = 10) littermates was not different. (**E**) Compared with *p*SENP1-WT mice (n = 11), *p*SENP1-KO (n = 9) mice were glucose intolerant following an oral glucose challenge. (**F**) Plasma insulin responses to oral glucose were blunted in *p*SENP1-KO mice (n = 6 of each genotype). Data are mean ± SEM and were compared with ANOVA followed by Bonferroni post-test or by 2-tailed Student's t test (AUC in **E** and **F**). $^*P < 0.05$, $^{**}P < 0.01$, $^{***}P < 0.001$.

mice. SENP1 was severely reduced in islets from either model (Figure 7B and Supplemental Figure 4A), while mRNA of other *Senp* isoforms was unchanged (Supplemental Figure 4B). SENP1 protein was low in mouse hypothalami (Supplemental Figure 4C), and the body weight of *p*SENP1-WT and *p*SENP1-KO animals did not differ (Figure 7C). Compared with littermate controls (*Senp1*$^{+/+}$ *Cre*$^+$ mice), the *p*SENP1-KO mice showed equivalent insulin tolerance (Figure 7D) but were intolerant of an oral glucose challenge at 6 (Supplemental Figure 4D) and 12 weeks (Figure 7E). Similar results were observed in the iβSENP1-KO mice (Supplemental Figure 4E). Heterozygous *Senp1*$^{fl/+}$ *Cre*$^+$ mice had an intermediate phenotype (Supplemental Figure 4, F and G). The plasma insulin response to oral glucose was reduced in *p*SENP1-KO mice (Figure 7F), despite the fact that islet morphology (Figure 8A) and α cell and β cell mass (Supplemental Figure 5A) were unchanged.

The secretory response of isolated *p*SENP1-KO islets to glucose and KCl was impaired (Figure 8B and Supplemental Figure 5B), as was the response to a protocol (9) assessing the K_{ATP}-independent amplification of insulin secretion (Figure 8C). The insulin content of islets from *p*SENP1-KO mice was unchanged (Supplemental Figure 5B). A similar phenotype was observed in islets from *i*βSENP1-KO mice (Supplemental Figure 5, C and D) or in response to acute knockdown of SENP1 achieved by treatment of *SENP1*$^{fl/fl}$ islets with an adenovirus expressing the Cre recombinase (Ad-Cre; Supplemental Figure 5, E and F).

In human β cells, knockdown of SENP1 had little effect on action potential dynamics (Supplemental Figure 6, A and B), while action potential firing was only modestly affected in *p*SENP1-KO β cells (Figure 8D and Supplemental Figure 6C). This is consistent with the SUMO-dependent regulation of Kv2.1 channels (Supplemental Figure 6D and ref. 36), which have a more prominent role in the control of electrical activity in mouse than in human β cells (51). Overall, however, this was not sufficient to alter the $[Ca^{2+}]_i$ responses in *p*SENP1-KO islets (Figure 8E). Rather, impaired insulin secretion results from an impaired glucose-dependent amplification of exocytosis that was rescued by reintroduction of cSENP1 via the patch pipette (Figure 8F). Mouse β cells lacking SENP1 also failed to respond to NADPH (Supplemental Figure 6D) and GSH (Figure 8G). Thus, a reduction of SENP1 in β cells causes glucose intolerance due to an impaired ability of glucose, and its downstream signals, to amplify insulin exocytosis.

Discussion

The canonical mechanism of glucose-stimulated insulin secretion involving increases in metabolism-derived ATP, inhibition of K_{ATP} channels, and activation of VDCCs was first introduced more than 30 years ago (3) and remains as a cornerstone mechanism for the "triggering" of insulin secretion. It is clear, however, that the K_{ATP} channel mechanism does not define the entire secretory response (9–11). Multiple metabolic coupling intermediates have been proposed as factors that amplify the secretory response to a triggering Ca^{2+} signal (13), with the net export of mitochondrial substrates and reducing equivalents being one strong candidate (19, 20). Here, we show that the glucose-dependent amplification of exocytosis in human β cells, which is disrupted in T2D, requires isocitrate flux through ICDc and the generation of cytosolic NADPH and GSH. These act through SENP1 to amplify the exocytosis of insulin, thereby controlling glucose homeostasis.

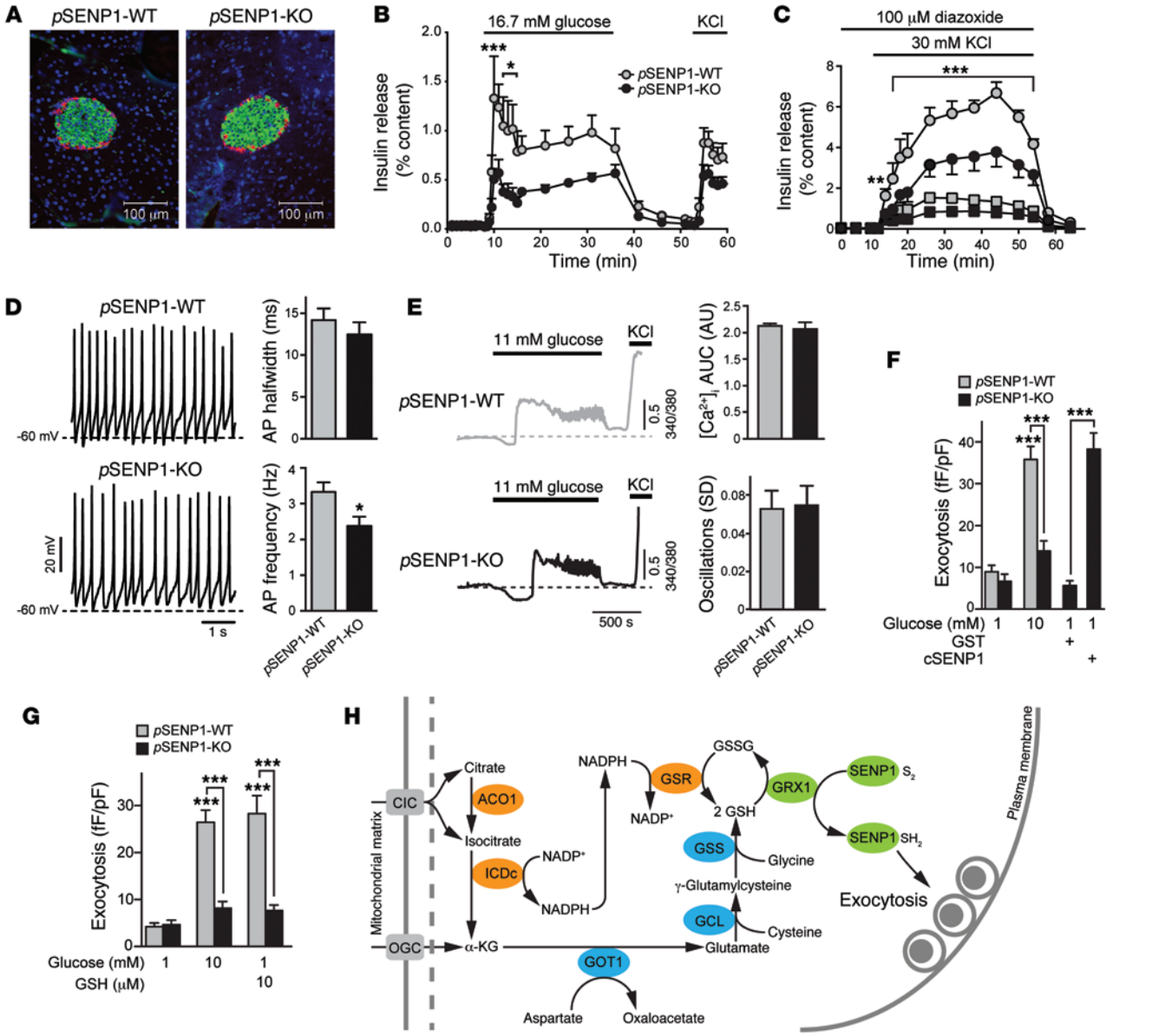

Figure 8. Pancreatic islet–specific knockout of *Senp1* blunts insulin secretion due to an impaired amplification of exocytosis. (**A**) Immunostaining of *p*SENP1-WT and *p*SENP1-KO mouse pancreatic sections for insulin (green), glucagon (red), and nuclei (blue) revealed no difference in islet architecture (see also Supplemental Figure 3B; $n = 4$ mice of each genotype). (**B**) Perifusion profile of the secretory response to glucose (16.7 mM) and KCl (30 mM) of *p*SENP1-WT and *p*SENP1-KO islets ($n = 4$ mice of each genotype). (**C**) With K_{ATP} channels held open with diazoxide, the secretory response of *p*SENP1-WT islets ($n = 4$ mice) to KCl (30 mM) at 16.7 mM (circles) versus 2.8 mM (squares) glucose is blunted in *p*SENP1-KO islets ($n = 4$ mice). (**D**) Action potential firing is moderately altered in *p*SENP1-KO β cells ($n = 17, 19$ cells; 3 and 4 mice of each genotype; see also Supplemental Figure 6, A–C), (**E**) although islet intracellular Ca^{2+} responses were unchanged ($n = 4$ mice of each genotype). (**F**) The glucose-dependent amplification of exocytosis is lost in *p*SENP1-KO β cells, and is rescued by reintroduction of cSENP1 (4 μg/ml; $n = 28, 33, 42, 32, 37, 39$ cells; 4 mice of each genotype). (**G**) GSH (10 μM) is unable to amplify exocytosis in *p*SENP1-KO β cells ($n = 37, 39, 57, 51, 32, 49$ cells; 5 mice of each genotype). (**H**) Proposed pathway linking mitochondrial export of (iso)citrate, glutathione biosynthesis (blue), and glutathione reduction (orange) pathways to the amplification of insulin exocytosis (yellow). Data are mean ± SEM and were compared with ANOVA followed by Bonferroni post-test (**B**, **C**, **F**, and **G**) or by 2-tailed Student's *t* test (**D** and **E**). $^*P < 0.05$, $^{***}P < 0.001$. Scale bar: 100 μm (**A**). *n* values correspond to graph bars from left to right, respectively.

Glucose affects the magnitude of subsequent secretory responses at concentrations below those required to trigger Ca^{2+} entry (9, 11). Indeed, the glucose-dependent amplification of exocytosis in human β cells is half maximal at approximately 4.5 mM, less than the corresponding value for inducing insulin secretion from human islets reported here and elsewhere (52, 53). This is consistent with the increased glucose oxidation in human islets at between 1 and 6 mM glucose (54) and suggests that glucose concentrations below the threshold for electrical activity and Ca^{2+} entry can determine the size of the secretory granule pool available for release. We show that this amplifying action of glucose is lost in β cells in an in vitro model of lipotoxicity and in β cells from

donors with T2D. This likely follows from the impaired glucose utilization (47), oxygen consumption (27, 54), and mitochondrial hyperpolarization (55) reported previously in islets from donors with T2D. Although one outcome of impaired mitochondrial function is reduced ATP generation (55), we found that the impairment of exocytosis in T2D β cells persists when intracellular ATP is high. This is consistent with the view that alternative metabolic coupling factors play a key role in the amplification of insulin secretion (13).

A variety of biochemical and molecular methods has led to evidence supporting a role for pyruvate carboxylase–mediated anaplerotic metabolism of glucose in insulin secretion (13, 19, 20) and the importance of isocitrate engagement with ICDc (22, 23). NADPH produced by this reaction is proposed to increase insulin exocytosis via GRX1 (24, 25). Consistent with this, we found that (a) isocitrate and NADPH were as potent as glucose in amplifying the exocytotic response, while the product of the ICDc reaction, α-KG, was ineffective; (b) siRNA-mediated suppression of ICDc blocked the glucose- and isocitrate-dependent amplification of exocytosis, an effect that could be rescued by NADPH; (c) NADH, an alternate source of reducing equivalents that does not engage with glutathione reductase, was unable to amplify exocytosis; and (d) this pathway connects to glutathione metabolism by maintaining glutathione synthesis and promoting glutathione reduction.

Although one recent study suggests little change in cytosolic GSH while mitochondrial GSH increases upon glucose stimulation of islets (41), we observed herein a reduction of the cytosolic GSH probe in human islets from several donors and a clear increase in total cellular GSH/GSSG ratio in response to stimulatory glucose in INS 832/13 cells that was blocked by knockdown of the cytosolic NADPH generating enzyme ICDc. Regardless, the ability of isocitrate to amplify exocytosis in T2D β cells, in which glucose stimulation failed, suggests that these cells have the functional machinery to transduce an isocitrate signal to amplify the exocytotic response. This is consistent with the ability of a membrane-permeable analog of malate, dimethylmalate, to restore glucose-stimulated insulin secretion in lipid-cultured INS 832/13 cells or in islets from Zucker diabetic fatty rats (56). This is likely due to provision of a source of pyruvate for anaplerotic metabolism, leading to export of citrate and isocitrate from the mitochondria.

Distal mediators of amplification of the insulin secretory response are not well described. Our previous work suggests that SUMOylation acts as a brake on insulin exocytosis, and a glucose-dependent deSUMOylation event at the exocytotic site is required for efficient insulin secretion (30). Intriguingly, the SUMO protease SENP1 (but not the closely related SENP2) is redox dependent (31), consistent with our observations that GSH and GRX1 can increase the activity of this enzyme. The redox sensitivity of SENP1 has been ascribed to key thiols on cysteine 603 (the catalytic residue conserved in all SENPs) and cysteine 613 (unique to SENP1 and SENP5), which we find are required for amplification of exocytosis. A role for the redox-dependent regulation of SENP1 is supported by the opposing actions of H_2O_2 and GSH/GRX1 on SENP1 activity observed in vitro and our previous finding that oxidation prevents the SENP1-dependent amplification of exocytosis (32).

SUMOylation is suggested to control the activity of the key β cell transcription factors MAFA and PDX1 (57, 58). However, insulin content and islet morphology are unchanged following knockout of SENP1, and thus, the acute nature by which cSENP1 affects the amplification of exocytosis suggests a direct, rather than transcriptionally mediated, role in insulin secretion. SUMOylation also controls GLP-1 receptor signaling (35), islet survival (37), and glucokinase activity (34). While a role for SENP1 per se (as opposed to other SENPs) in these contexts remains to be investigated, here we have demonstrated a key role for SENP1 in the amplification of insulin exocytosis to control glucose homeostasis in four different models of SENP1 deficiency: by acute knockdown with siRNA in human β cells and by transduction of mouse *Senp1*$^{fl/fl}$ β cells with Ad-Cre and in both tissue-selective (pSENP1-KO) and tissue-inducible (*i*βSENP1-KO) mouse models. The exact mechanism by which SENP1 augments the distal exocytotic response remains an area of investigation, and several proteins involved in granule trafficking and exocytosis are subject to posttranslational SUMOylation (30, 36, 59–62). We demonstrated previously the glucose-dependent deSUMOylation of synaptotagmin VII (30). DeSUMOylation of synaptotagmin VII is maximal at 15 minutes after glucose stimulation, consistent with the time course of glucose-stimulated SENP1 reduction and SUMO protease activity observed in the present study. Whether deSUMOylation of synaptotagmin VII alone can account for amplification of insulin exocytosis remains unclear; it is likely that SENP1 acts on multiple targets within the exocytotic machinery. Regardless, SENP1 appears to act very near the exocytotic site, given its ability to colocalize with membrane-associated secretory granules and our previous observation that upregulation of SUMO1 blocks exocytosis downstream of insulin granule recruitment.

Thus, we propose (Figure 8H) that glucose stimulation amplifies the secretory response through a pathway that requires the ICDc-dependent generation of NADPH and GSH, which is coupled to enhanced Ca^{2+}-dependent exocytosis by SENP1. Impairment of this signaling pathway in T2D could occur in several ways: (a) reduced mitochondrial function, leading to lowered isocitrate export and cytosolic NADPH production; (b) oxidative stress and redirection of NADPH, GSH, and GRX1 into a protective function; or (c) direct oxidative inactivation of SENP1 (32). That dysfunction in β cells from donors with T2D can be circumvented by reintroduction of isocitrate-to-SENP1 pathway intermediates suggests that the exocytotic mechanism remains intact and could be harnessed for alternative therapeutic approaches to increase insulin secretion in T2D.

Methods

Pancreatic islet isolation and cell culture. Human islets were isolated from donor pancreata at the Alberta Diabetes Institute IsletCore (http://www.bcell.org/IsletCore.html) or the Clinical Islet Laboratory at the University of Alberta as previously described (63) and cultured in low-glucose (5.5 mM) DMEM with L-glutamine, 110 mg/l sodium pyruvate, 10% FBS, and 100 U/ml penicillin/streptomycin. In total, islets from 99 human donors were examined in this study (Supplemental Tables 1 and 2). Diabetes status was determined by patient clinical history and in one case by HbA1c measurement (we took >7.0% HbA1c as indicative of T2D). Mouse islets were isolated by collagenase digestion and cultured in RPMI-1640 containing 11.1 mM glucose with 10% FBS and 100 U/ml penicillin/streptomycin. In all experiments, islets were handpicked for purity. For single-cell experiments, islets were

dissociated in Ca^{2+}-free buffer, plated in 35-mm dishes, and cultured overnight. INS 832/13 cells were cultured in RPMI-1640 containing 11.1 mM glucose with 10% FBS, 10 mM HEPES, 0.29 mg/ml L-glutamine, 1 mM sodium pyruvate, 50 μM β-mercaptoethanol, and 100 U/ml penicillin/streptomycin, as described previously (64).

Transgenic animals. An ES cell–targeting vector containing exons 14 and 15 flanked by loxP sequence was generated with a neomycin cassette flanked with FRT sequence at the 3′-adjacent region. This was transfected/electroporated into ES cells. The positive ES cells were determined by PCR/Southern blot and then injected into C57BL/6 mice to generate chimeric mice. Mice containing Loxp and Neo were crossed with FLP-FRT mice in order to delete neomycin. Mice containing Loxp without Neo were crossed with *Pdx1-Cre* mice (49) on a C57BL/6 background [B6.FVB-Tg(Pdx1-cre)6Tuv/J] and *Pdx1-CreER* mice (50) on a C56BL/6 background [Tg(Pdx1-Cre/Esr1*)#Dam/J] from The Jackson Laboratory. Experiments were performed on male littermates between 6 and 14 weeks of age as indicated. Ear notches were used to determine mice genotypes by using the REDExtract-N-Amp Tissue PCR Kit (Sigma-Aldrich) and primers listed in Supplemental Table 3. At 10 weeks, $Senp1^{fl/fl}$ × *Pdx-CreER* mice and control littermates were injected 3 times with 225 mg/kg tamoxifen prepared in corn oil every 2 days.

Recombinant proteins and plasmid constructs. cSENP1 was from Enzo Life Technologies. Recombinant GRX1 and glutathione-*S*-transferase were from Abcam. Flag-SENP1 was from Addgene (plasmid 17357). Flag-SENP1 mutants were generated by site-directed mutagenesis followed by Dpn1 digestion using primers listed in Supplemental Table 3. The mutagenesis was confirmed by Sanger sequencing. pEGFP-SENP1 plasmid was generated by cloning the SENP1 cDNA sequence from Flag-SENP1 plasmid into pEGFP backbone (Clontech) using Bgl II and Sal I restriction enzymes (New England Biolabs). Plasmids were transfected in INS 832/13 cells and dissociated human islet cells with Lipofectamine 2000 (Life Technologies).

Recombinant adenoviruses. Recombinant adenoviruses used to suppress the expression of ICDc (Ad-shICDc) in INS 832/13 cells or deliver a scrambled control shRNA (Ad-shScrambled) were described previously (23, 65). Adenoviruses expressing GFP (Ad-GFP), Cre-IRES-GFP (Ad-Cre), and GFP-SENP1 (Ad-GFP-SENP1) were from Welgen Inc. Intact and dissociated islets were infected with recombinant viruses as previously described (66).

siRNA-mediated knockdown and quantitative PCR. Sequences and suppliers for siRNA duplexes used are presented in Supplemental Table 3. These were transfected in dissociated human islet cells or INS 832/13 cells using DharmaFECT 1 (GE Healthcare). For quantitative PCR, RNA was extracted using TRIzol Reagent (Life Technologies). cDNA was synthesized using Super Script II and oligodT (Life Technologies) according to the manufacturer's protocol. Real-time PCR was performed as previously described (37) using primers listed in Supplemental Table 3.

Chemical reagents. Unless stated otherwise, all chemical reagents were from Sigma-Aldrich. Fatty acid–free BSA was from Roche. Fatty acid stock solution was prepared as follows. Oleate and palmitate were dissolved at 70°C in 150 mM NaCl to final concentrations of 13.5 and 6.6 mM, respectively. Fatty acid complexation was achieved by dissolving 1 volume of the previous solution in 1 volume of free fatty acid BSA (8.35% in 150 mM NaCl) at 37°C with stirring for an hour. The stock solution was diluted 10 times in culture media with 1% FBS for a final concentration of 400 μM free fatty acid.

Single-cell measurement of β cell exocytosis, action potentials, and currents. Prior to patch-clamping, dissociated islet cells or INS 832/13 cells were preincubated in DMEM (human) or RPMI-1640 (mouse and INS 832/13) media with 1 mM glucose for 1 hour. Media were then changed to bath solution containing 118 mM NaCl, 20 mM TEA, 5.6 mM KCl, 1.2 mM $MgCl_2 \cdot 6H_2O$, 2.6 mM $CaCl_2$, 5 mM HEPES, and either 1 mM or 10 mM glucose (pH 7.4 with NaOH) in a heated chamber (32°C–35°C). After approximately 15 minutes in the bath solution, whole-cell patch-clamp measurement of exocytosis was performed (30). The intracellular solution contained 125 mM Cs-glutamate, 10 mM CsCl, 10 mM NaCl, 1 mM $MgCl_2 \cdot 6H_2O$, 0.05 mM EGTA, 5 mM HEPES, 0.1 mM cAMP, and 3 mM MgATP (pH 7.15 with CsOH), and compounds or recombinant enzymes were added to this as indicated for dialysis into the cell. In one set of experiments (Figure 2G), cAMP was omitted and the concentration of MgATP was 0.3 mM. When NADPH or NADH were used, these were 100 μM together with 10 μM of $NADP^+$ or NAD^+, respectively. Exocytosis was stimulated by activating VDCCs with a series of membrane depolarizations from –70 to 0 mV.

Action potentials and voltage-dependent K^+ currents were measured essentially as described previously (67) using the amphotericin perforated-patch and whole-cell configurations, respectively. Cells were preincubated and then treated with 10 mM glucose as described above for the exocytosis measurements. Following all patch-clamp experiments, cells were positively identified as β cells by insulin immunostaining. Capacitance responses (fF) and K^+ current (pA) were normalized to initial cell size in picofarad (pF).

Measurement of insulin secretion. Insulin secretion was measured in static secretion assays as described previously (30) or by perifusion at 37°C in Krebs-Ringer buffer (KRB) (115 mM NaCl, 5 mM KCl, 24 mM $NaHCO_3$, 2.5 mM $CaCl_2$, 1 mM $MgCl_2$, 10 mM HEPES, and 0.1% BSA, PH 7.4). For static incubations, 15 handpicked islets were preincubated for 2 hours in 1 mM glucose KRB prior to a 1-hour test period in the same solution, followed by a 1-hour test period in 16.7 mM glucose KRB. For perifusion, 20 islets per lane were perifused (0.1 ml/min) with 2.8 mM glucose KRB for 30 minutes and then with the indicated condition. Islets were lysed in acid/ethanol buffer (1.5% concentrated HCl, 23.5% acetic acid, and 75% ethanol) for total insulin content. Samples were assayed using the Insulin Detection Kit (Meso Scale Discovery).

Glucose and insulin tolerance. Mice were fasted for 4 hours with free access to water. At 6 and 12 weeks, glucose tolerance test was assessed after oral administration of 1 g/kg dextrose by gavage. Blood was collected at the indicated times in Microvette 100 Li Heparin (Sarstedt) and centrifuged at 4°C for 10 minutes at 9,330 *g*. Supernatant was collected to measure serum insulin with the Insulin Detection Kit (Meso Scale Discovery). At 14 weeks, insulin tolerance was assessed after intraperitoneal injection of 1 U/kg Humulin R (Eli Lilly).

Imaging. For immunofluorescence of pancreatic sections, pancreata were fixed with Z-fix (VWR Canada) and embedded in paraffin with sections stained as previously described (68). The total pancreatic section was imaged as a mosaic with a Zeiss Axio Observer.Z1 microscope and ×40 Plan Ap°Chromat objective (1.4 NA). Excitation was with a COLIBRI (Carl Zeiss Canada) LED light source with 350-, 495-, or 555-nm filter set. Insulin- and glucagon-positive areas were quantified with ImageJ software (NIH Image). The β and α cell mass were determined as the relative insulin- and glucagon-positive area from 3 to 7 sections of each pancreas normalized to pancreas weight.

Dissociated human islets and INS 832/13 cells cultured on coverslips were fixed with Z-fix and stained with rabbit polyclonal SENP1 antibody (Acris, AP06456PU, dilution 1:50) overnight at room temperature. Cells were then stained with the guinea pig polyclonal insulin antibody (Dako, A0564, dilution 1:500) for 1 hour at room temperature. Afterward, the Alexa Fluor 594 anti-rabbit (Life Technologies, A-11037) and Alexa Fluor 488 anti–guinea pig (Life Technologies, A-11073) secondary antibodies were applied for an hour. Then, coverslips were mounted with the Prolong Gold Antifade Mountant with DAPI (Life Technologies), and images were acquired using an Olympus AIVI Spinning Disc confocal microscope with a 100× objective. Colocalization was measured using Volocity 3D Image Analysis Software (PerkinElmer).

For total internal reflection fluorescence (TIRF) imaging, INS 832/13 cells were transfected with pEGFP-SENP1 and pmCherry-IAPP plasmids using Lipofectamine 2000 (Life Technologies) and fixed with Z-fix after 48 hours. Imaging was performed with a Cell-TIRF motorized TIRF system (Olympus Canada) equipped with a 100×/1.49 NA TIRFM objective, a Photometrics Evolve 512 camera (Photometrics), and Metamorph Imaging software (Molecular Devices). Stimulation wavelengths were 491 nm and 561 nm, and the penetration depth was set to 105 nm. Colocalization was analyzed with ImageJ (NIH Image) using the JaCoP colocalization plugin.

Calcium imaging of intact mouse islets was performed as previously described (30) using Fura2-AM (Life Technologies).

Fluorescent biosensor measurement of glutathione redox state. A fusion protein (Grx1-roGFP) of cytosolic GRX1 and redox-sensitive GFP (roGFP) (69) was transduced into dispersed human islet cells using an adenoviral vector at an MOI of 200 particles per cell. The cells were then reaggregated (5,000 cells per reaggregated islet) by centrifugation at 1,643 *g* in a 96-well V-bottom plate and cultured for 3 days before being transferred to glass-bottom confocal dishes in 1 mM glucose Krebs buffer. Islets were imaged after a 30-minute preincubation in this buffer and then the glucose concentration was increased to 10 mM before imaging 20 minutes after this addition. For normalization, the fully reduced state was achieved by addition of 5 mM DTT for 15 minutes; the fully oxidized state was achieved by addition of 0.5 mM diamide for 10 minutes. We then performed a Wilcoxon (nonparametric, paired) test for significance in which islets from each donor were aggregated and each donor was treated as an *n* value.

Glutathione measurement by HPLC. 72 hours after transfection with siScrambled or siICDc duplexes, confluent plates of INS 832/13 cells were preincubated for 1.5 hours in KRB containing 2.5 mM glucose, followed by incubation for an additional 20 minutes with either 2.5 or 12 mM glucose. Cells were washed, lifted, pelleted, and resuspended in 500 μl homogenization buffer containing 50 mM Trizma base supplemented with 20 mM boric acid, 20 mM L-serine, 20 μM acivicin to inhibit γ-glutamyltranspeptidase, and 5 mM N-ethylmaleimide. The 500-μl cell suspension was snap frozen for lysis. The cell homogenate was thawed on wet ice and split into 2 derivatization pathways for the measurement of GSH and GSSG using HPLC (70, 71). For GSH derivatization, 150 μl of the homogenate was added to 100 μl of 60% trichloroacetic acid to deproteinize the sample, vortexed, and then centrifuged for 5 minutes at 20,000 *g*. The supernatant was transferred to an autosampler vial for HPLC.

GSH samples were run on freshly made mobile phase consisting of a 0.25% glacial acetic acid mixed directly with 6% HPLC grade acetonitrile. Samples were analyzed using a Shimadzu Prominence HPLC system equipped with a Purospher STAR RP-18 endcapped column (4.6 × 150 mm; 3 μm, EMD Millipore) at flow rate of 0.5 ml/min. GSH–N-ethylmaleimide conjugate was detected by UV chromatography at a wavelength of 265 nm (Shimadzu SPD-20A) (71). For GSSG derivatization, 150 μl of the cell homogenate was deproteinized in 200 μl of 15% perchloric acid, vortexed, and then centrifuged for 5 minutes at 20,000 *g*. The resulting supernatant (200 μl) was next diluted in 1 ml of 0.1 M NaOH twice to pH 12 before reacting with 0.1% o-phthaladehyde to form a fluorescent product detectable at excitation/emission wavelengths of 350/420 nm (Shimadzu RF-20A xs) (70). Derivatized GSSG samples were processed using a 25 mM sodium phosphate buffer containing 15% HPLC-grade methanol at pH 6 and run through a Shimadzu Prominence HPLC system equipped with the same column described above at flow rate of 0.5 ml/min. All samples were quantified using standards prepared under identical conditions and normalized to the protein content measured in the INS 832/13 homogenate by BCA assay.

Measurement of amino acid levels by targeted tandem mass spectrometry. INS 832/13 insulinoma cells, cultured in 6-well plates, were preincubated for 1.5 hours in secretion buffer containing 114 mM NaCl, 4.7 mM KCl, 1.2 mM KH_2PO_4, 1.16 mM $MgSO_4$, 20 mM HEPES, and 2.5 mM $CaCl_2$, with 0.2% BSA (pH 7.2), containing 2.5 mM glucose, followed by incubation in secretion buffer for an additional 2 hours with either 2.5 or 12 mM glucose. When indicated, the general transaminase inhibitor aminooxyacetic acid was present at 10 mM during both the preincubation and incubation. Cells were washed 3 times with cold PBS, quick frozen on the plate, and sonicated in H_2O on ice. Amino acid levels were measured in the cleared lysates by tandem mass spectrometry as described previously (72, 73).

SUMO protease activity. INS 832/13 cells were preincubated for 3 hours in culture media with 1 mM glucose and for an additional hour in KRB with 1 mM glucose. Cells were then incubated for the indicated time with 10 mM glucose KRB and then lysed in 1x passive lysis buffer (Promega). A fraction of cell extract was added to 500 nM SUMO1-AMC substrate (Enzo Life Science), and fluorescence was monitored over 5 minutes (380 nm excitation, 515 nm emission) using the Wallac Evasion plate reader (Perkin Elmer). Protein concentration was determined by BCA protein assay (Piercenet).

For in vitro SENP1 activity, human GRX1 (10 μg/ml, Abcam) and GSH (10 μM, Sigma-Aldrich) were incubated with cSENP1 (50 μM, Boston Biochem) in a buffer containing 20 mM Tris-HCl, 20 mm NaCl, pH 7.8. AMC release reaction was initiated by adding 1 μM SUMO1-AMC (Boston Biochem). Release of AMC fluorescence was monitored by fluorimetry, with 380 nm excitation and 460 nm emission wavelengths. The fluorescence reading was recorded with the Synergy 2 Multi-Mode Plate Reader from BioTek for 30 minutes with 1-minute intervals at room temperature.

Western blotting and pull-down experiments. For standard Western blotting, rabbit polyclonal SENP1 antibody (1:2,000) was provided by Mary Dasso (NIH, Bethesda, Maryland, USA) (74). Mouse β-actin antibody (1:1,000) was from Santa Cruz Biotechnology Inc. (sc-47778). Cells were harvested and then lysed in RIPA lysis buffer. Whole-cell lysates were separated using SDS-PAGE, transferred to PVDF membrane, and probed with indicated antibodies.

The thiol groups (or sulfhydryl groups) on Flag-SENP1 expressed in INS 832/13 cells were labeled with biotin using 2.5 μM EZ-Link BMCC-biotin (Thermo Scientific) for 1 hour at 4°C. The biotinylated

Flag-SENP1 was captured with streptavidin-agarose (Thermo Scientific) overnight at 4°C; eluted using 6 M guanidine HCl and 0.1 M glycine, pH 2.5; and subsequently precipitated by methanol chloroform precipitation. The pellet was dissolved in SDS-PAGE loading buffer, and the biotinylated SENP1 was quantified by Western blot using a mouse monoclonal SENP1 antibody (1:500) from Santa Cruz Biotechnology Inc. (sc-271360).

Statistics. Data analysis was performed using FitMaster (HEKA Electronik) and GraphPad Prism (v6.0c). All data are shown as the mean, and error bars represent SEM. For exocytosis data only, statistical outliers were identified by an unbiased ROUT (robust regression followed by outlier identification) test (75) and removed from subsequent analyses. Comparison of multiple groups was performed using ANOVA followed by Bonferroni post-test or the nonparametric Kruskal-Wallis 1-way ANOVA followed by Dunn's post-test. When comparing two means only, data were analyzed by the 2-tailed Student's *t* test or nonparametric Wilcoxon analysis. A *P* value less than 0.05 was considered significant.

Study approval. All animal and human islet studies were approved by the Animal Care and Use Committee (AUP00000291, AUP00000405) and the Human Research Ethics Board (Pro00001754) at the University of Alberta. All families of organ donors provided informed consent for use of pancreatic tissue in research.

Acknowledgments

We thank the Human Organ Procurement and Exchange program and the Trillium Gift of Life Network for their efforts in obtaining human organs for transplantation and research. We also thank James Lyon from the Alberta Diabetes Institute IsletCore and James Shapiro and Tatsuya Kin from the Clinical Islet Transplant program at the University of Alberta for human islet isolations. We are grateful to James Johnson (University of British Columbia) for advice on mouse models and to Mary Dasso (NIH) for providing SENP1 antibody. Funding for human islet isolation was provided by the Alberta Diabetes Foundation (ADF) and the University of Alberta to P.E. MacDonald. This research was funded by a grant from the Canadian Institutes of Health Research (CIHR) (MOP244739) to P.E. MacDonald and a grant from the NIH (DK42538) to C.B. Newgard and by an islet metabolism consortium grant to R.G. Kibbey, O. Shirihai, C.B. Newgard, and P.E. MacDonald from Pfizer Inc. M. Ferdaoussi held a fellowship from the ADF. J.P. Mackay holds studentships from the CIHR and Alberta Innovates — Health Solutions. A.L. Gloyn is a Wellcome Trust Senior Fellow in Basic Biomedical Research (095101/Z/10/Z). W.F. Colmers is a Medical Scientist of the Alberta Heritage Foundation for Medical Research. E.T.H. Yeh holds the Ting Tsung and Wei Fong Chao Distinguished Chair. P.E. MacDonald holds a Canada Research Chair in Islet Biology.

Address correspondence to: Patrick E. MacDonald, University of Alberta, Alberta Diabetes Institute, LKS Centre, Rm. 6-126, Edmonton, Alberta, Canada, T6G 2E1. Phone: 780.492.8063; E-mail: pmacdonald@ualberta.ca. Or to: Christopher B. Newgard, Duke Molecular Physiology Institute, Duke University Medical Center, 300 North Duke St., Durham, North Carolina 27701, USA. Phone: 919.668.6059; E-mail: chris.newgard@duke.edu. Or to: Edward T.H. Yeh, Department of Cardiology, The University of Texas MD Anderson Cancer Center, 1400 Pressler St., Unit 1451, Houston, Texas 77030, USA. Phone: 713.792.1960; E-mail: etyeh@mdanderson.org.

1. Kahn SE, Cooper ME, Del Prato S. Pathophysiology and treatment of type 2 diabetes: perspectives on the past, present, and future. *Lancet*. 2014;383(9922):1068–1083.
2. Henquin JC. Regulation of insulin secretion: a matter of phase control and amplitude modulation. *Diabetologia*. 2009;52(5):739–751.
3. Ashcroft FM, Harrison DE, Ashcroft SJ. Glucose induces closure of single potassium channels in isolated rat pancreatic β-cells. *Nature*. 1984;312(5993):446–448.
4. Rorsman P, Trube G. Glucose dependent K^+-channels in pancreatic β-cells are regulated by intracellular ATP. *Pflugers Arch*. 1985;405(4):305–309.
5. Dean PM, Matthews EK. Electrical activity in pancreatic islet cells. *Nature*. 1968;219(5152):389–390.
6. Satin LS, Cook DL. Voltage-gated Ca^{2+} current in pancreatic B-cells. *Pflugers Arch*. 1985;404(4):385–387.
7. Orci L, Amherdt M, Malaisse-Lagae F, Rouiller C, Renold AE. Insulin release by emiocytosis: demonstration with freeze-etching technique. *Science*. 1973;179(4068):82–84.
8. Pace CS, Tarvin JT, Neighbors AS, Pirkle JA, Greider MH. Use of a high voltage technique to determine the molecular requirements for exocytosis in islet cells. *Diabetes*. 1980;29(11):911–918.
9. Gembal M, Gilon P, Henquin JC. Evidence that glucose can control insulin release independently from its action on ATP-sensitive K^+ channels in mouse B cells. *J Clin Invest*. 1992;89(4):1288–1295.
10. Sato Y, Aizawa T, Komatsu M, Okada N, Yamada T. Dual functional role of membrane depolarization/Ca^{2+} influx in rat pancreatic B-cell. *Diabetes*. 1992;41(4):438–443.
11. Henquin JC. Triggering and amplifying pathways of regulation of insulin secretion by glucose. *Diabetes*. 2000;49(11):1751–1760.
12. Macdonald PE. Signal integration at the level of ion channel and exocytotic function in pancreatic β-cells. *Am J Physiol Endocrinol Metab*. 2011;301(6):E1065–E1069.
13. Prentki M, Matschinsky FM, Madiraju SRM. Metabolic signaling in fuel-induced insulin secretion. *Cell Metab*. 2013;18(2):162–185.
14. Henquin JC. The dual control of insulin secretion by glucose involves triggering and amplifying pathways in β-cells. *Diabetes Res Clin Pract*. 2011;93(suppl 1):S27–S31.
15. Prentki M, Madiraju SRM. Glycerolipid/free fatty acid cycle and islet β-cell function in health, obesity and diabetes. *Mol Cell Endocrinol*. 2012;353(1–2):88–100.
16. Zhao S, et al. α/β-Hydrolase domain-6-accessible monoacylglycerol controls glucose-stimulated insulin secretion. *Cell Metab*. 2014;19(6):993–1007.
17. Kibbey RG, Pongratz RL, Romanelli AJ, Wollheim CB, Cline GW, Shulman GI. Mitochondrial GTP regulates glucose-stimulated insulin secretion. *Cell Metab*. 2007;5(4):253–264.
18. Stark R, et al. Phosphoenolpyruvate cycling via mitochondrial phosphoenolpyruvate carboxykinase links anaplerosis and mitochondrial GTP with insulin secretion. *J Biol Chem*. 2009;284(39):26578–26590.
19. Jensen MV, Joseph JW, Ronnebaum SM, Burgess SC, Sherry AD, Newgard CB. Metabolic cycling in control of glucose-stimulated insulin secretion. *Am J Physiol Endocrinol Metab*. 2008;295(6):E1287–E1297.
20. Lu D, et al. ^{13}C NMR isotopomer analysis reveals a connection between pyruvate cycling and glucose-stimulated insulin secretion (GSIS). *Proc Natl Acad Sci U S A*. 2002;99(5):2708–2713.
21. Guay C, et al. A role for cytosolic isocitrate dehydrogenase as a negative regulator of glucose signaling for insulin secretion in pancreatic β-cells. *PLoS One*. 2013;8(10):e77097.
22. Joseph JW, et al. The mitochondrial citrate/isocitrate carrier plays a regulatory role in glucose-stimulated insulin secretion. *J Biol Chem*. 2006;281(47):35624–35632.
23. Ronnebaum SM, et al. A pyruvate cycling pathway involving cytosolic NADP-dependent isocitrate dehydrogenase regulates glucose-stimulated insulin secretion. *J Biol Chem*. 2006;281(41):30593–30602.
24. Reinbothe TM, et al. Glutaredoxin-1 mediates NADPH-dependent stimulation of calcium-

dependent insulin secretion. *Mol Endocrinol*. 2009;23(6):893–900.
25. Ivarsson R, et al. Redox control of exocytosis: regulatory role of NADPH, thioredoxin, and glutaredoxin. *Diabetes*. 2005;54(7):2132–2142.
26. Marchetti P, et al. Pancreatic islets from type 2 diabetic patients have functional defects and increased apoptosis that are ameliorated by metformin. *J Clin Endocrinol Metab*. 2004;89(11):5535–5541.
27. Del Guerra S, et al. Functional and molecular defects of pancreatic islets in human type 2 diabetes. *Diabetes*. 2005;54(3):727–735.
28. Anello M, et al. Functional and morphological alterations of mitochondria in pancreatic β cells from type 2 diabetic patients. *Diabetologia*. 2005;48(2):282–289.
29. Yeh ET. SUMOylation and De-SUMOylation: wrestling with life's processes. *J Biol Chem*. 2009;284(13):8223–8227.
30. Dai XQ, et al. SUMOylation regulates insulin exocytosis downstream of secretory granule docking in rodents and humans. *Diabetes*. 2011;60(3):838–847.
31. Xu Z, Lam LS, Lam LH, Chau SF, Ng TB, Au SW. Molecular basis of the redox regulation of SUMO proteases: a protective mechanism of intermolecular disulfide linkage against irreversible sulfhydryl oxidation. *FASEB J*. 2008;22(1):127–137.
32. Vergari E, Plummer G, Dai XQ, MacDonald PE. DeSUMOylation controls insulin exocytosis in response to metabolic signals. *Biomolecules*. 2012;2(2):269–281.
33. Manning Fox JE, Hajmrle C, Macdonald PE. Novel roles of SUMO in pancreatic β-cells: thinking outside the nucleus. *Can J Physiol Pharmacol*. 2012;90(6):765–770.
34. Aukrust I, et al. SUMOylation of pancreatic glucokinase regulates its cellular stability and activity. *J Biol Chem*. 2013;288(8):5951–5962.
35. Rajan S, Torres J, Thompson MS, Philipson LH. SUMO downregulates GLP-1-stimulated cAMP generation and insulin secretion. *Am J Physiol Endocrinol Metab*. 2012;302(6):E714–E723.
36. Dai XQ, Kolic J, Marchi P, Sipione S, Macdonald PE. SUMOylation regulates Kv2.1 and modulates pancreatic β-cell excitability. *J Cell Sci*. 2009;122(pt 6):775–779.
37. Hajmrle C, et al. SUMOylation protects against IL-1β-induced apoptosis in INS-1 832/13 and human islets. *Am J Physiol Endocrinol Metab*. 2014;307(8):E664–E673.
38. Eliasson L, Renström E, Ding WG, Proks P, Rorsman P. Rapid ATP-dependent priming of secretory granules precedes Ca(2+)-induced exocytosis in mouse pancreatic B-cells. *J Physiol (Lond)*. 1997;503(pt 2):399–412.
39. Worthington DJ, Rosemeyer MA. Glutathione reductase from human erythrocytes. Catalytic properties and aggregation. *Eur J Biochem*. 1976;67(1):231–238.
40. Staal GE, Veeger C. The reaction mechanism of glutathione reductase from human erythrocytes. *Biochim Biophys Acta*. 1969;185(1):49–62.
41. Takahashi HK, et al. Acute nutrient regulation of the mitochondrial glutathione redox state in pancreatic β-cells. *Biochem J*. 2014;460(3):411–423.
42. Maechler P, Wollheim CB. Mitochondrial glutamate acts as a messenger in glucose-induced insulin exocytosis. *Nature*. 1999;402(6762):685–689.
43. Bailey D, O'Hare P. Characterization of the localization and proteolytic activity of the SUMO-specific protease, SENP1. *J Biol Chem*. 2004;279(1):692–703.
44. Hoppa MB, et al. Chronic palmitate exposure inhibits insulin secretion by dissociation of Ca(2+) channels from secretory granules. *Cell Metab*. 2009;10(6):455–465.
45. Collins SC, et al. Progression of diet-induced diabetes in C57BL6J mice involves functional dissociation of Ca2(+) channels from secretory vesicles. *Diabetes*. 2010;59(5):1192–1201.
46. Ostenson CG, Gaisano H, Sheu L, Tibell A, Bartfai T. Impaired gene and protein expression of exocytotic soluble N-ethylmaleimide attachment protein receptor complex proteins in pancreatic islets of type 2 diabetic patients. *Diabetes*. 2006;55(2):435–440.
47. Fernandez-Alvarez J, Conget I, Rasschaert J, Sener A, Gomis R, Malaisse WJ. Enzymatic, metabolic and secretory patterns in human islets of type 2 (non-insulin-dependent) diabetic patients. *Diabetologia*. 1994;37(2):177–181.
48. Vernier S, et al. β-Cell metabolic alterations under chronic nutrient overload in rat and human islets. *Islets*. 2012;4(6):379–392.
49. Hingorani SR, et al. Preinvasive and invasive ductal pancreatic cancer and its early detection in the mouse. *Cancer Cell*. 2003;4(6):437–450.
50. Gu G, Dubauskaite J, Melton DA. Direct evidence for the pancreatic lineage: NGN3+ cells are islet progenitors and are distinct from duct progenitors. *Development*. 2002;129(10):2447–2457.
51. Braun M, et al. Voltage-gated ion channels in human pancreatic β-cells: electrophysiological characterization and role in insulin secretion. *Diabetes*. 2008;57(6):1618–1628.
52. Henquin JC, Dufrane D, Nenquin M. Nutrient control of insulin secretion in isolated normal human islets. *Diabetes*. 2006;55(12):3470–3477.
53. Harrison DE, Christie MR, Gray DW. Properties of isolated human islets of Langerhans: insulin secretion, glucose oxidation and protein phosphorylation. *Diabetologia*. 1985;28(2):99–103.
54. Doliba NM, et al. Glucokinase activation repairs defective bioenergetics of islets of Langerhans isolated from type 2 diabetics. *Am J Physiol Endocrinol Metab*. 2012;302(1):E87–E102.
55. Anello M, Gilon P, Henquin JC. Alterations of insulin secretion from mouse islets treated with sulphonylureas: perturbations of Ca^{2+} regulation prevail over changes in insulin content. *Br J Pharmacol*. 1999;127(8):1883–1891.
56. Boucher A, et al. Biochemical mechanism of lipid-induced impairment of glucose-stimulated insulin secretion and reversal with a malate analogue. *J Biol Chem*. 2004;279(26):27263–27271.
57. Kanai K, et al. SUMOylation negatively regulates transcriptional and oncogenic activities of MafA. *Genes Cells*. 2010;15(9):971–982.
58. Kishi A, Nakamura T, Nishio Y, Maegawa H, Kashiwagi A. Sumoylation of Pdx1 is associated with its nuclear localization and insulin gene activation. *Am J Physiol Endocrinol Metab*. 2003;284(4):E830–E840.
59. Geerts CJ, Jacobsen L, van de Bospoort R, Verhage M, Groffen AJA. Tomosyn interacts with the SUMO E3 ligase PIASγ. *PLoS One*. 2014;9(3):e91697.
60. Girach F, Craig TJ, Rocca DL, Henley JM. RIM1α SUMOylation is required for fast synaptic vesicle exocytosis. *Cell Rep*. 2013;5(5):1294–1301.
61. Castillo-Lluva S, et al. SUMOylation of the GTPase Rac1 is required for optimal cell migration. *Nat Cell Biol*. 2010;12(11):1078–1085.
62. Plant LD, Dowdell EJ, Dementieva IS, Marks JD, Goldstein SA. SUMO modification of cell surface Kv2.1 potassium channels regulates the activity of rat hippocampal neurons. *J Gen Physiol*. 2011;137(5):441–454.
63. Kin T, Shapiro AM. Surgical aspects of human islet isolation. *Islets*. 2010;2(5):265–273.
64. Hohmeier HE, Newgard CB. Cell lines derived from pancreatic islets. *Mol Cell Endocrinol*. 2004;228(1–2):121–128.
65. Ronnebaum SM, et al. Silencing of cytosolic or mitochondrial isoforms of malic enzyme has no effect on glucose-stimulated insulin secretion from rodent islets. *J Biol Chem*. 2008;283(43):28909–28917.
66. Ferdaoussi M, et al. G protein-coupled receptor (GPR)40-dependent potentiation of insulin secretion in mouse islets is mediated by protein kinase D1. *Diabetologia*. 2012;55(10):2682–2692.
67. Spigelman AF, Dai X, Macdonald PE. Voltage-dependent K(+) channels are positive regulators of alpha cell action potential generation and glucagon secretion in mice and humans. *Diabetologia*. 2010;53(9):1917–1926.
68. Manning Fox JE, et al. Functional plasticity of the human infant β-cell exocytotic phenotype. *Endocrinology*. 2013;154(4):1392–1399.
69. Gutscher M, et al. Real-time imaging of the intracellular glutathione redox potential. *Nat Methods*. 2008;5(6):553–559.
70. Kand'ár R, Záková P, Lotková H, Kucera O, Cervinková Z. Determination of reduced and oxidized glutathione in biological samples using liquid chromatography with fluorimetric detection. *J Pharm Biomed Anal*. 2007;43(4):1382–1387.
71. Giustarini D, Dalle-Donne I, Milzani A, Fanti P, Rossi R. Analysis of GSH and GSSG after derivatization with N-ethylmaleimide. *Nat Protoc*. 2013;8(9):1660–1669.
72. An J, et al. Hepatic expression of malonyl-CoA decarboxylase reverses muscle, liver and whole-animal insulin resistance. *Nat Med*. 2004;10(3):268–274.
73. Wu JY, et al. ENU mutagenesis identifies mice with mitochondrial branched-chain aminotransferase deficiency resembling human maple syrup urine disease. *J Clin Invest*. 2004;113(3):434–440.
74. Chow KH, Elgort S, Dasso M, Ullman KS. Two distinct sites in Nup153 mediate interaction with the SUMO proteases SENP1 and SENP2. *Nucleus*. 2012;3(4):349–358.
75. Motulsky HJ, Brown RE. Detecting outliers when fitting data with nonlinear regression — a new method based on robust nonlinear regression and the false discovery rate. *BMC Bioinformatics*. 2006;7:123.